Icarus 420 (2024) 116189

Contents lists available at ScienceDirect

Icarus

journal homepage: www.elsevier.com/locate/icarus

Micro-FTIR reflectance spectroscopy of Ryugu, CI chondrites and volatile-rich clasts – Comparing spectral features in the Mid-IR (2.5–16.5 μm) region

J. Storz [a], M.P. Reitze [a], A.N. Stojic [a,*], I. Kerraouch [a,b], A. Bischoff [a], H. Hiesinger [a], T. John [c]

[a] Institut für Planetologie, University of Münster, Wilhelm-Klemm-Str. 10, D-48149 Münster, Germany.
[b] Buseck Center for Meteorite Studies (BCMS), Arizona State University, Tempe, AZ 85827, USA.
[c] Freie Universität Berlin, Institut für Geologische Wissenschaften, Malteserstr. 74-100, D-12249 Berlin, Germany.

ARTICLE INFO

Keywords:
Asteroid Ryugu
Carbonaceous chondrites
Infrared spectroscopy
Mineralogy

ABSTRACT

Although C1 clasts in carbonaceous chondrites are usually mineralogically similar to CI chondrites, they often exhibit distinct chemical or isotope characteristics, indicating that the diversity of carbonaceous matter is larger than represented by currently known meteorites. Samples returned by the Hayabusa2 mission provide an excellent opportunity to directly compare remote sensing data with laboratory spectra and elaborate on meteorite-asteroid links.

We obtained reflectance spectra from 10 carbonaceous samples of extraterrestrial origin to identify spectral differences in the wavelength region between 2.5 and 16.5 μm. We investigated seven volatile-rich clasts, two CI chondrites, and a fragment from the asteroid Ryugu, recently returned by the Hayabusa2 mission. To obtain representative spectra from a lithology, we performed multiple analysis with an aperture size of 100 μm × 100 μm. Subsequently, spectral features were correlated with petrographic and chemical data.

The phyllosilicate composition of the investigated C1 and C2 clasts is on average more Fe-rich compared to bulk CI chondrites, which is spectrally reflected in lower Christiansen feature (CF)/Reststrahlenband (RB) ratios. Our results confirm previous studies that indicate that the band area of the OH absorption band at 2.7 μm is dependent on the phyllosilicate composition. A high Mg abundance in phyllosilicates leads to a stronger OH absorption band. Varying degrees of aqueous alteration cause mineralogic differences that are observable in the reflectance spectra. Either in form of a band center shift towards smaller or longer wavelengths, depending on the metal cation giving rise to the M-OH absorption band, and/or a generally weaker OH absorption band, and a broad Reststrahlen band (RB) at 10 μm, with two minor RBs emerging at 11.3 and 12 μm. In contrast, most C1 clasts show a single RB at ≈10 μm, and a constant OH band position at 2.70 μm. The abundance of minor constituents, such as sulfides and carbonates, can also affect the spectrum. Dolomite produces two diagnostic bands at 6.5 and 11.3 μm, whereas pyrrhotite, devoid of diagnostic bands in this wavelength region, increases the background while decreasing the RB intensity.

Our findings indicate that within a laboratory framework, subtle mineralogic differences among hydrated carbonaceous materials can be spectroscopically detected. The spectra of Ryugu sample A0008 show a distinctive OH absorption band, as seen in the globally retrieved data by the NIRS3 instrument for Ryugu (Kitazato et al., 2019). Under specific circumstances, micro-FTIR reflectance spectra can be qualitatively compared to remote sensing spectra, and help to further elaborate on meteorite-asteroid links.

1. Introduction

IR spectroscopy is one of the most important tools in planetary science to investigate planetary surfaces. One key advantage of IR reflectance spectroscopy is that material properties can be determined via remote sensing, and by comparison with known endmembers, spectral features can be linked to mineralogy. Conventionally, the visible and near-infrared (VNIR) range of the electromagnetic spectrum

* Corresponding author.
E-mail address: A.stojic@uni-muenster.de (A.N. Stojic).

https://doi.org/10.1016/j.icarus.2024.116189
Received 28 February 2024; Received in revised form 11 June 2024; Accepted 11 June 2024
Available online 13 June 2024

Table 1
Extracted variables from averaged reflectance spectra of Ryugu, CI chondrites, and C1/C2 clasts.

						OH band				
IRIS ID	Sample	Type	Clast type	Section ID	n=	Center	Area (cm^{-1})	FWHM (cm^{-1})	CF position	RB position
477	Ryugu	Asteroid	–	A0008A2	16	2.70 ± 0.86%	0.13	34	9.05	10.01
478	Orgueil	CI1	–	PL23012	5	2.70 ± 0.57%	0.11	33	9.02	9.92
479	Ivuna	CI1	–	PL23011	5	2.70 ± 0.60%	0.15	37	9.05	9.91
481	Acfer 97	CR2	C1	PL92521	5	2.71 ± 0.58%	0.49	47	8.85	9.78
484	Acfer 187	CR2	C1	PL91023	4	2.71 ± 2.06%	0.36	45	8.83	9.82
487	Acfer 182	CH3	C1	PL01266	5	2.71 ± 1.26%	0.22	40	9.00	9.95
489	Acfer 207	CH3	C1	PL91162	5	2.71 ± 0.99%	0.26	37	9.00	9.97
486	Acfer 214	CH3	C1	PL92271	5	2.71 ± 0.52%	0.62	41	8.89	9.97
488	Sahara 98645	H3	C1/C2	PL99062	4	2.71 ± 2.10%	0.15	55	8.88	9.88
485	DaG 319	Ureilite	C2	PL17084	4	2.73 ± 3.07%	0.14	98	8.85	9.97

has been used for asteroid taxonomy and meteorite-asteroid links (e.g., Tedesco et al., 1989; Tholen, 1989; Tholen and Barucci, 1989; Xu et al., 1995; Bus and Binzel, 2002; DeMeo et al., 2009). However, recently more studies have been conducted for the mid-IR (MIR) range (e.g., Lim et al., 2005; Osawa et al., 2005; Emery et al., 2006; Takir and Emery, 2012; King et al., 2015; Vernazza et al., 2015; Morlok et al., 2020; Skulteti et al., 2020), as this wavelength region is sensitive to fundamental molecular vibrations of Si—O modes in particular, and therefore expected to be more diagnostic of mineralogy.

It is estimated that a fraction of about 53% of the main belt mass is populated by C-complex asteroids (DeMeo and Carry, 2013), which have been related to hydrated carbonaceous chondrites (Gaffey et al., 1993; Takir et al., 2015; DeMeo et al., 2022). This indicates that hydrated CC meteorites, such as CI and CM chondrites, are significantly underrepresented in the terrestrial meteorite inventory. CI chondrites are very rare and of particular importance in geo- and cosmochemistry, as they are the most primitive materials in terms of element abundances (Lodders, 2003; Palme et al., 2014). All CI chondrites have experienced strong aqueous alteration (petrologic type 1), and impact brecciation on their parent bodies (e.g., Tomeoka and Buseck, 1988; Morlok et al., 2006a; Alfing et al., 2019). CI chondrites contain significant amounts of water (up to 10 wt%) in form of hydrated, hydroxylated or oxyhydroxylated components (Brearley, 2006). As such, CI chondrites have been frequently discussed as a source for the volatile element inventory of terrestrial planets (e.g., Schönbächler et al., 2010; Marty et al., 2013; Braukmüller et al., 2019; Greenwood et al., 2023).

Aqueously altered CI and CM chondrites are known to contain several characteristic spectral features in the mid-IR region (Beck et al., 2010; Beck et al., 2014; Bates et al., 2020; Morlok et al., 2020; Hiroi et al., 2021). The most prominent features are the Christiansen feature (CF), the Reststrahlen bands (RBs), and the H_2O/OH absorption bands. The CF occurs between 7.5 and 9 μm, and is a point of minimum reflectance, regarded as indicative of mineral composition (Conel, 1969; Salisbury et al., 1991). The RBs are located between 8.5 and 12 μm and are caused by fundamental molecular vibrations of silicates (Salisbury et al., 1991). At ≈3 μm fundamental O—H stretching vibrations associated with hydrated silicates occur (Salisbury et al., 1991; Miyamoto and Zolensky, 1994), more specifically the M-OH bond produces a band at 2.7 μm. Also contributing in this spectral area are fundamental vibrational bands related to the asymmetric and symmetric stretching motions of the H_2O molecule.

Samples returned by the Hayabusa2 mission from C-type asteroid 16173 Ryugu, provide an excellent opportunity to directly compare remote sensing data with in situ acquired spectra from the laboratory, potentially allowing for a more definitive link between asteroids and meteorites.

First results of the Hayabusa2 mission indicated that Ryugu is composed of material similar to CC meteorites, and that the surface is highly porous and dominated by loosely gravitationally bound boulders, rather than centimeter-sized regolith as previously anticipated (Kitazato et al., 2019; Sugita et al., 2019; Grott et al., 2020; Sakatani et al., 2021). MIR spectra obtained by the MARA instrument (4 channels in the 5.5–15.5 μm range), which is part of the MASCOT lander, support a CC origin and highlight that Ryugu experienced strong aqueous alteration (Hamm et al., 2022). Hamm et al. (2022) analyzed multiple thin sections of CC meteorites, and found that the best spectral match for Ryugu was obtained by CI chondrites. In December 2020, the sample return capsule of the Hayabusa2 mission successfully returned asteroid samples to Earth (Morota et al., 2020; Yada et al., 2022). First studies of the returned samples confirmed the link between Ryugu and CI chondrites (Greenwood et al., 2023; Nakamura et al., 2023; Yokoyama et al., 2023).

Primitive volatile-rich matter, analogous to CI chondrites, has been found in several meteorites as xenoliths (i.e., clasts), including CR, CH, CB, OC, HED, and ureilites (e.g., Bischoff et al., 1993a, 1993b; Endreß et al., 1994; Zolensky et al., 1996; Briani et al., 2012; Bischoff et al., 2018; Patzek et al., 2018; Goodrich et al., 2019). These volatile-rich clasts bear significant amounts of aqueous alteration-related minerals such as phyllosilicates, carbonates, and magnetite. However, some clasts have distinct chemical or isotope characteristics, including phyllosilicate chemistry and H-, O-, and S-isotope composition (e.g., Patzek et al., 2018; Visser et al., 2019; Patzek et al., 2020; Kerraouch et al., 2022). Therefore, the term C1 clasts is often preferred in the recent literature, emphasizing that these xenoliths are not necessarily identical with CI chondrites. These results imply that the diversity of C1 material is larger than represented by currently known meteorites. Volatile-rich clasts, which do not correspond to known meteorites, can provide insights into yet unsampled aqueously altered parent bodies.

One major aim of this study is to determine whether C1 clasts are spectroscopically distinct from CI chondrites. As most clasts are very small and embedded in thin sections, micro-FTIR is an excellent technique to obtain spectral data, otherwise not possible for this sample type. We also obtained spectra of Ryugu sample A0008, allowing us to correlate in situ measured spectra with remote sensing data. We specifically paid attention to intra-sample heterogeneity, as Ryugu sample A0008 shows a brecciated texture. With the acquired spectral dataset we identified similarities and differences between the investigated carbonaceous samples. Additionally, we tried to identify the causes of spectral differences by comparing spectral information with mineralogy.

2. Methods

2.1. Samples

For in situ analyses, newly prepared polished thick sections (section A0008A2 from sample cut A0008A) of Ryugu sample A0008, and the CI chondrites Ivuna and Orgueil were used. The Ryugu sample was collected at the first touchdown site on the asteroid (sample chamber A). Additionally, polished thin sections of seven volatile-rich clasts embedded in seven different meteorites were analyzed. The samples include two paired CR chondrites (Acfer 079 and Acfer 187), three paired CH chondrites (Acfer 182, Acfer 207, and Acfer 214), one ureilite (Dar al Gani (DaG) 319), and one H chondrite (Sahara 98,645). The

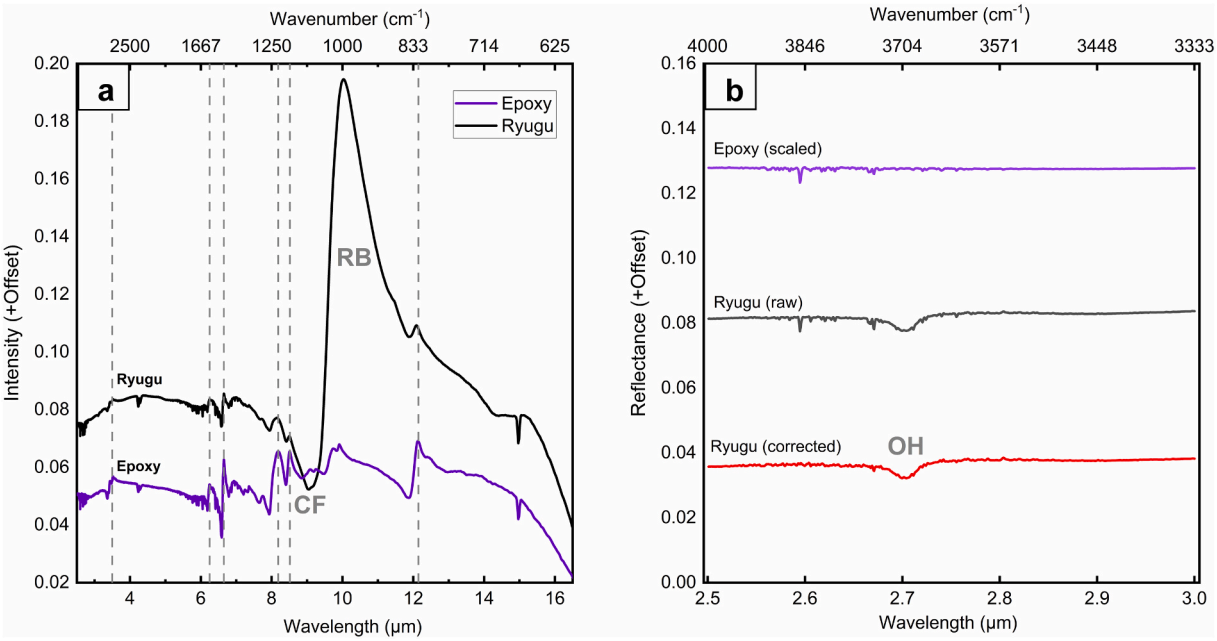

Fig. 1. (a) Influence of epoxy resin on the Ryugu spectrum. Epoxy manifests itself in several features in the spectrum, particularly <9 μm. The dotted lines indicate several areas where epoxy shows strong features. The RB and CF are unaffected. (b) Raw spectra of epoxy and Ryugu, and the effect of epoxy signal removal. Epoxy shows absorption features related to CH-stretching in the 2.7 μm region, however, it does not display a genuine OH absorption band. The subtraction of the epoxy-related absorption features improves the spectral quality, while retaining the genuine position and shape of the OH absorption band, providing the basis for the peak fitting procedure.

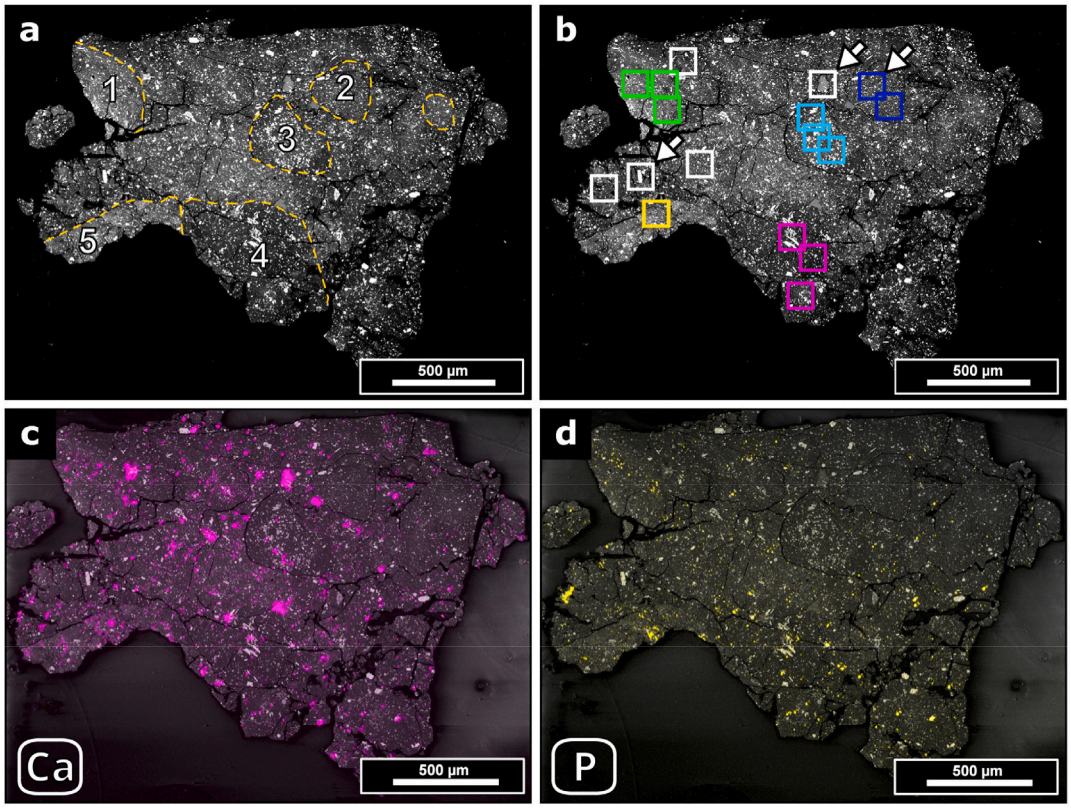

Fig. 2. BSE images of Ryugu sample A0008: (a) The sample shows a brecciated texture and several clasts are marked by dashed lines. The numbers of the clasts correspond to the clasts average spectra shown in Fig. 8. (b). The colored squares represent FTIR measurement sites of the clasts.: green = clast 1, dark blue = clast 2, light blue = clast 3, purple = clast 4, yellow = clast 5. The size of the squares is equivalent to the size of the aperture used. The arrows mark the location of spectra presented in Fig. 9. (c,d) Elemental maps of Ryugu showing the distribution of (c) Ca (purple) and (d) P (yellow). (For interpretation of the references to colour in this figure legend, the reader is referred to the web version of this article.)

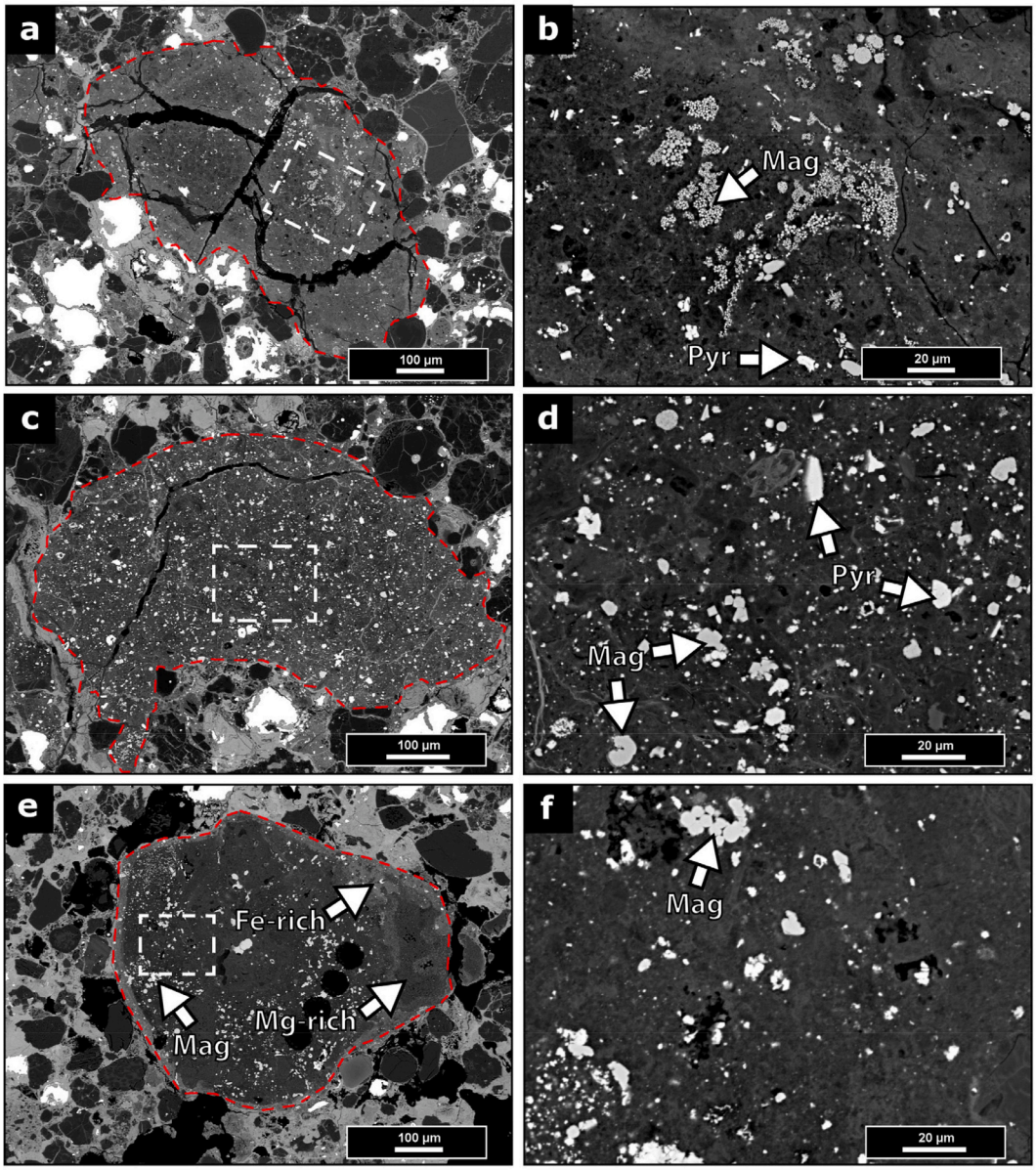

Fig. 3. BSE images of the investigated C1 clasts in the CH meteorites (a,b) Acfer 182 (c,d) Acfer 207 and (e,f) Acfer 214. The clast boundaries are represented by red dashed lines. The dashed rectangles indicate the location for the images seen on the right side (b,d,f). The arrows aid phase identification in the Figure: Mag = Magnetite, Pyr = Pyrrhotite, Fe-rich = Fe-rich phyllosilicates, Mg-rich = Mg-rich phyllosilicates. (For interpretation of the references to colour in this figure legend, the reader is referred to the web version of this article.)

Ryugu sample was prepared at the Tohoku University after the procedure by Nakashima et al. (2023). All other samples were prepared at the University of Münster.

2.2. Micro-FTIR

The IR reflectance spectra were obtained with a Bruker Hyperion 3000 FT-IR microscope coupled to a Bruker Vertex 80v at ambient conditions. The device is located at the Infrared and Raman for Interplanetary Spectroscopy (IRIS) laboratory at the University of Münster. The liquid nitrogen-cooled mercury-cadmium-tellurium (MCT) detector measures in the electromagnetic range between 2.5 and 16.7 µm. The microscope and sample chamber were purged with dry air to minimize atmospheric interferences. The spectra were obtained using a 15× Cassegrain objective, and an aperture size of 100 µm × 100 µm. A polished gold mirror was used for calibration. The analyses were integrated over 512 scans. Ryugu, Ivuna, and Orgueil were measured with a spectral resolution of 2 cm^{-1}. For the volatile-rich clasts a spectral resolution of 4 cm^{-1} was used. The obtained spectral data are available in the MERTIS Infrared and Raman for Interplanetary Spectroscopy (IRIS) database, using the IDs presented in Table 1.

For extracting the band position of maximum (RB) and minimum (CF) reflectance, the raw spectra were smoothed with an adjacent-averaging algorithm (moving window of 10), which is a simple and subtle smoothing method. As the region from 2.5 to 3 µm usually showed a poor signal-to-noise ratio, it was isolated and smoothed with a more potent locally weighted least squares second-order polynomial regression algorithm (Loess) with a span of 0.2. This method provided the best results in retaining the shape of the OH band, while eliminating noise (cf. Fig. 1b). The area and the full width at half maximum (FWHM) of the OH band were extracted by plotting a straight baseline (range between 2.6 and 2.8 µm) and applying a Gaussian peak fit.

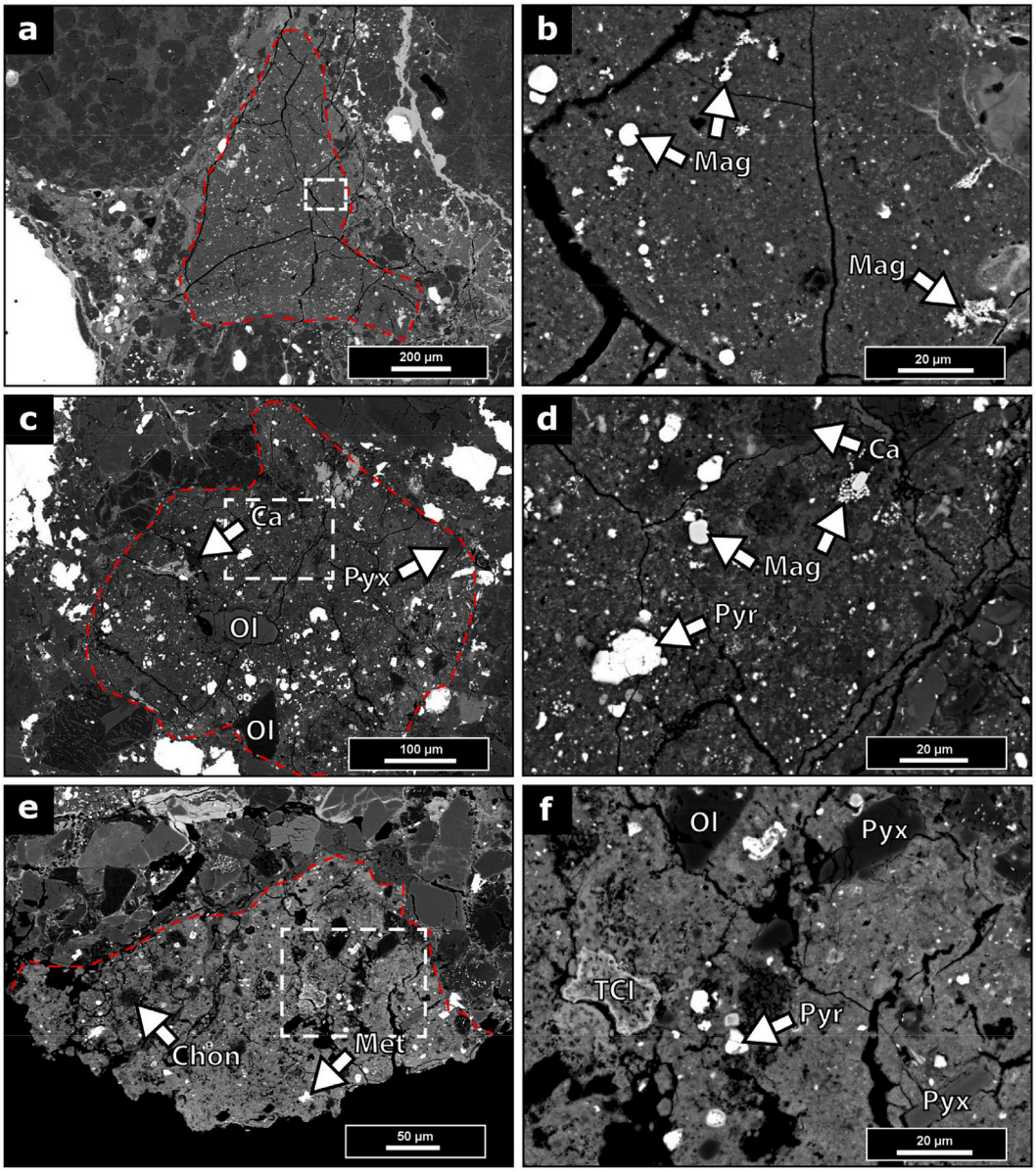

Fig. 4. Backscatter electron (BSE) images of C1/C2 clasts in (a,b) Acfer 097 (CR2), (c,d) Sahara 98645 (H3), and (e,f) DaG 319 (ureilite). The clast boundaries are represented by dashed red lines. The dashed rectangles indicate the location of the images seen on the right side (b,d,f). The arrows aid phase identification in the Figure: Ol = Olivine, Pyx = Pyroxene, Mag = Magnetite, Pyr = Pyrrhotite, Ca = Carbonate, Met = Fe-Ni metal, TCI = tochilinite-cronstedtite intergrowth, Chon = Chondrule. (For interpretation of the references to colour in this figure legend, the reader is referred to the web version of this article.)

2.3. SEM-EDX

For imaging and elemental analysis, a JEOL 6610-LV scanning electron microscope (SEM) was used. The device is located at the Interdisciplinary Center for Electron Microscopy (ICEM) at the University of Münster. For energy-dispersive X-ray spectroscopy (EDS) the INCA software provided by Oxford Instruments was used. For EDS calibration, natural and synthetic standards by Astimex Standards Ltd. were used. The device was operated with an excitation voltage of 20 kV and a probe current of 1.5 nA.

3. Results

3.1. Petrography

3.1.1. Ryugu & CI Chondrites

Optical inspection and SEM analysis reveal that Ryugu sample A0008A consists primarily of a fine-grained phyllosilicate-bearing matrix, which occupies >90 vol% of the section. The sample is brecciated and several clasts are visible (Fig. 2a). The friable and highly porous nature of this material leads to abundant cracks throughout the section. The matrix also contains small sub-micrometer sized magnetite and sulfide grains. Clast 2 shows a particularly high matrix abundance compared to the bulk sample (Fig. 2a). Magnetite and pyrrhotite are also present as larger grains (>10 µm), sometimes forming local enrichments as in clast 3 (Fig. 2a), which contains abundant magnetite grains with a plaquette morphology. Large pyrrhotite grains often form laths as seen in clast 4 and site of interest M5 (Fig. 2a,b). Magnetite grains are mostly compact, but also occur as framboids or spherules throughout the section. Carbonates are predominately present as dolomite, and tend to form large irregularly-shaped grains (Fig. 2a). The P element map also indicates a minor phosphate abundance (Fig. 2d). Overall, the mineralogy and the brecciated texture closely resembles CI chondrites. Comparing the here investigated samples, the texture and mineral

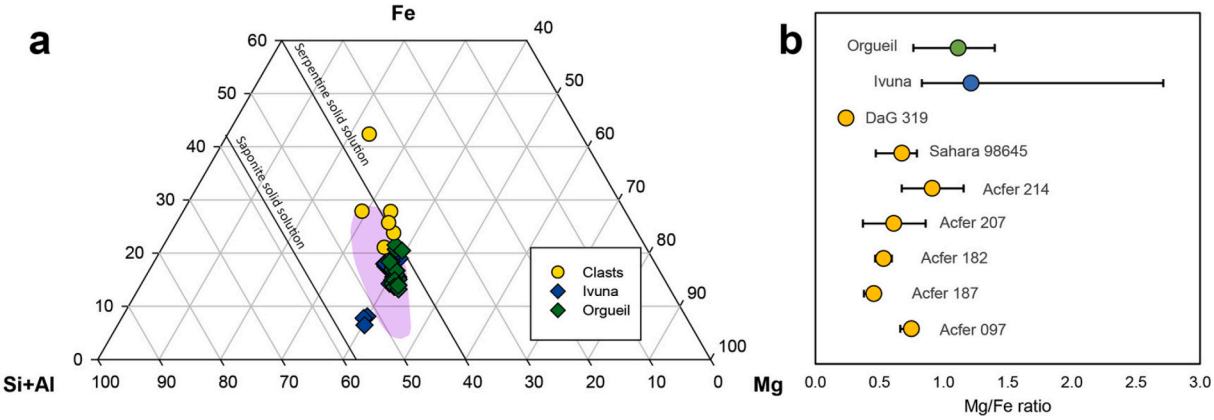

Fig. 5. (a) Ternary diagram displaying the phyllosilicate composition of Ivuna (blue), Orgueil (green), Ryugu (purple field), and the average of each clast (yellow). Ryugu field based on data from Yokoyama et al. (2023). (b) Average Mg/Fe ratio of phyllosilicates with range indicated by error bars. Of all measurements, the clasts show a smaller variability in their given Mg/Fe ratio than CI chondrites that exhibit a much greater Mg/Fe ratio range. C1 clasts in the studied CR chondrites seem to be particularly homogeneous. (For interpretation of the references to colour in this figure legend, the reader is referred to the web version of this article.)

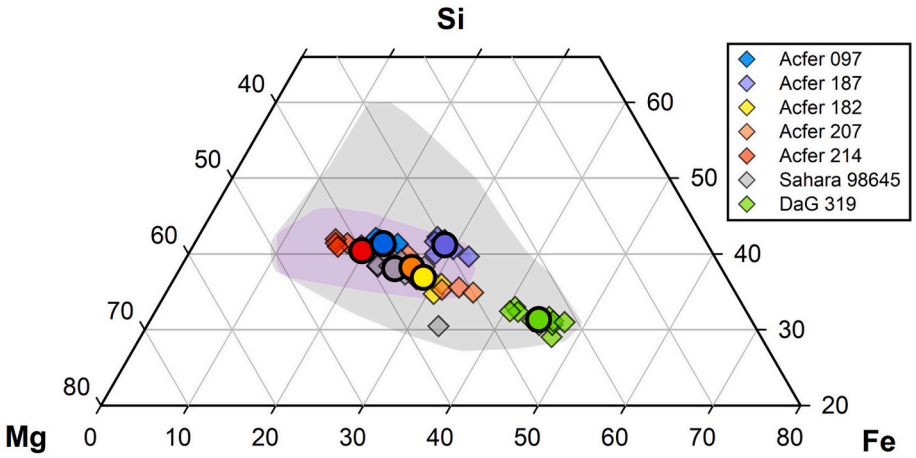

Fig. 6. Ternary diagram showing the Si, Mg, and Fe phyllosilicate composition of each clast. The average is displayed in circles, individual analyses in diamond shape. The grey area shows the typical range observed for CI-like clasts in ureilites, the purple area for CI-like clasts in CH/CR/CH chondrites. Fields based on data from Patzek et al. (2018). (For interpretation of the references to colour in this figure legend, the reader is referred to the web version of this article.)

distribution of Ryugu is most similar to Orgueil. Ivuna and Orgueil, are mainly composed of saponite and serpentine minerals, which is reflected in their chemical composition. The phyllosilicate composition of Ryugu, Ivuna, and Orgueil shows substantial overlap (Fig. 5).

3.1.2. C1/C2 Clasts

The clasts are texturally distinct from the host rock and often show abundant cracks. The size of the clasts is variable, ranging from 580 μm (Sahara 98645) to 3.5 mm (Acfer 187) in diameter. A fine-grained phyllosilicate-rich matrix is the major constituent in all clasts. Typical minor constituents include magnetite grains, mostly of spherical or framboid texture, and sulfide grains of compact and irregular shape. Sulfide grains are mostly pyrrhotite, and to a minor extend pentlandite. Locally, intergrowths of pyrrhotite and pentlandite are present. The abundance of magnetite and sulfides is highly variable among the clasts. For instance, the clast in Acfer 097 contains abundant magnetite and is almost free of sulfide grains, whereas it is reversed for the C1 clasts in Sahara 98645. Yet, most clasts show both minerals as minor constituents, as seen in CI chondrites. Porous and phyllosilicate-rich samples have analytical totals below 100 wt% in SEM-EDX and microprobe analyses (EPMA) due to the occurrence of cracks in the analyzed areas and the water-content of the high abundance of phyllosilicates (Fig. 3).

In some clasts, carbonates and phosphates are present as accessory phases.

Compared to other C1 clasts in this study, the clast in Sahara 98645 contains more olivine and pyroxene grains (Fig. 4). Also, the rim region is not as sharp as in the other clasts, as some larger grains from the host rock penetrate the clast boundary. While pyrrhotite and pentlandite are abundant, magnetite grains are rare. This indicates that aqueous alteration is not as advanced as in the other C1 clasts samples. The large olivine (Fa_{20}) in the center of the clast spans 120 μm in diameter. The other olivine grains are almost pure forsterite ($Fo_{>98}$). The phyllosilicate composition among the C1 clasts is quite similar, but on average Fe- and Si-richer compared to phyllosilicates in CI chondrites (Fig. 5).

The C2 clast in DaG 319 is distinct from the others clasts (Fig. 4e,f). Angular olivine ($Fo_{>95}$) and pyroxene grains are abundant. Kamacite and compact and irregular pyrrhotite grains are also present. Additionally, a fibrous tochilinite-cronstedtite-intergrowth (TCI), and an intact porphyritic-olivine-pyroxene (POP) chondrule are embedded in the matrix. The phyllosilicates are Fe-richer, which makes them stand out from C1 clasts and CI chondrites (Figs. 5,6). These mineralogic characteristics indicate that the clast experienced aqueous alteration to a significantly lesser degree. The C2 clast is petrographically more similar to CM2 chondrites than CI1 chondrites.

Table 2
Extracted variables from spectra obtained in different clasts of Ryugu A0008 (cf. Fig. 2a).

	OH band				
Lithology	Center	Area (cm^{-1})	FWHM (cm^{-1})	CF position	RB position
Clast 1	2.70 ± 1.05%	0.12	35	9.04	10.01
Clast 2	2.70 ± 0.85%	0.14	32	9.06	10.00
Clast 3	2.70 ± 0.79%	0.09	30	9.02	10.00
Clast 4	2.70 ± 1.37%	0.14	24	9.03	10.01
Clast 5	2.70 ± 0.67%	0.09	42	9.03	10.00

3.2. Spectra

All obtained spectra show a prominent Reststrahlen band (RB) at ≈10 μm, and a reflectance minimum at ≈9 μm, corresponding to the Christiansen feature (CF). These features are linked to mineralogy and silicate composition (e.g., Salisbury et al., 1991). Some spectra additionally show a shoulder at 10.8 μm, which is developed to varying degrees. Another prominent feature is the absorption band at 2.7 μm, associated with M-OH bond stretching vibrations in Mg-rich phyllosilicates (Beck et al., 2010; Takir et al., 2013).

Table 1 shows that the most variable features are the integrated water band area (0.09 to 0.62), followed by the CF (8.8 to 9.1 μm), and the RB position (9.8 to 10 μm). The band center of the OH band and its FWHM are almost constant. The only exception is the C2 clast in DaG 319, which shows a band center value of 2.73 μm. In Fig. 11, the most variable parameters are plotted against the Fe/Mg ratio of the phyllosilicates. It displays a weakly linear correlation between CF/RB ratio and the Mg/Fe ratio, with Acfer 214 being an outlier within the displayed ranges.

3.2.1. Ryugu & CI Chondrites

All 17 spectra obtained at 4 different sites of interest in Ryugu A0008 (Fig. 2b) show similar spectral features with a prominent RB at 10 μm, a pronounced CF at 9 μm, and an absorption band at 2.7 μm. One exception is a spectrum from site of interest M3 (cf. Fig. 2b), where a large carbonate grain produced two additional bands at 6.5 μm and 11.3 μm (Fig. 9b). These bands are associated with vibrational modes, asymmetric stretching (6.5 μm) and out-of-plane bending of the C—O bond (11.3 μm) of carbonate anions (Lane and Christensen, 1997). Although Ryugu contains different lithologies, the obtained spectra exhibit only small variability, especially in terms of band positions (Table 2). More subtle differences are still present (Fig. 8b), mostly in form of a variable shoulder at 10.8 μm. The magnetite-rich clast 3 shows a clear shoulder at 10.8 μm, contrasting to clast 1 and clast 5 (Fig. 8b).

Fig. 9 displays spectra from selected measurement sites, which are enriched in a specific mineral (cf. Fig. 2). The averaged Ryugu spectrum (of 16 analysis) is plotted for comparison. At first glance, the average spectrum of Ryugu resembles the phyllosilicate-rich spectrum the most, especially in terms of absorption intensity of the 2.7 μm band. In the sulfide-rich region, the depth of the OH absorption band is less pronounced, and shifted to shorter wavelengths. Additionally, the region between 2.8 and 3 μm shows a steeper slope. In the spectrum of the carbonate-rich region, the absorption of the 2.7 band is also decreased, but no peak shift is present. Compared to the phyllosilicate-rich spectrum, the average Ryugu spectrum also shows a weakly positive slope between 2.8 and 3 μm. This indicates that minor constituents like sulfides have subtle effects on the spectrum, although no diagnostic bands are present.

Fig. 9b displays the spectra in the wavelength region from 3 to 16.5 μm, and compares them with mineral endmembers taken form the RELAB database. The spectrum of the carbonate-rich region shows two additional bands at 6.5 and 11.3 μm. By comparison with the dolomite reference spectrum, and considering the Ca elemental map (Fig. 2c), the grain can be identified as dolomite. Yet, the signature of phyllosilicates is still strong in the spectrum, indicated by a prominent RB at 10 μm. The other Ruygu spectra show identical features in this wavelength region, although the spectrum of the sulfide-rich region shows a decreased RB intensity, and an increased background.

All Ryugu spectra show a peak at 12 μm, which is related to epoxy (Fig. 1a). This also applies to the less developed bands between 3.5 and 8.5 μm. The absorption band at 15 μm is related to atmospheric CO_2. As these bands are artifacts, they will not be further discussed. Overall, the spectra of Ryugu are quite similar to spectra from Ivuna and Orgueil. Compared to CI chondrites, the RBs of Ryugu are broader and more symmetric. Ivuna and Orgueil show a more pronounced shoulder at 10.8 μm, and a less pronounced reflectance minimum. In comparison, Ivuna shows an overall increased RB, and an additional small band at 9.2 μm.

3.2.2. C1/C2 Clasts

All clasts show a prominent RB, with band positions ranging from 9.8 to 10.0 μm (Fig. 10b). The CF ranges from 8.8 to 9.0 μm. The shoulder of the RB band at 10.8 μm is significantly less pronounced in all clasts compared to CI chondrites. The development of the OH band varies considerably (Fig. 10a). While Acfer 214 and Acfer 097 show a clear OH band as seen in Ryugu and CI chondrites, the OH band is very subtle and of different shape for the clasts in Sahara 98645 and DaG 319. The position of the OH band is relatively constant with an average of 2.7 μm, except for the C2 clast in DaG 319 (Table 1). The clasts from the CR chondrites show the highest reflectance intensity, followed by the clasts in CH chondrites. The intensity of the RB band is significantly lower in the C1/2 clast in Sahara 98645 and the C2 clast in DaG 319. This feature correlates with a weaker development of the OH band (Fig. 10). The C2 clast in DaG 319 shows two additional shoulders at 11.3 μm and 12 μm. These are most likely caused by two emerging RBs, indicative of olivine (Lane et al., 2011). The clasts in Sahara 98645 and Acfer 207 show two bands of minor intensity at 7.1 and 11.4 μm. The band at 11.4 μm is also likely related to olivine.

4. Discussion

First, we will discuss to what extent the sample mineralogy can be inferred from the acquired MIR spectra, as this is a fundamental constraint regarding meteorite-asteroid links based on spectroscopy. Second, we will evaluate similarities and differences between the investigated samples. Lastly, we will discuss whether micro-FTIR spectra provide valuable insights in the context of meteorite-asteroid links, also with respect to non-compositional effects.

4.1. Correlating spectra with mineralogy

In the investigated samples, the phyllosilicate-rich matrix usually accounts for >90 vol% of the sample, and has therefore a major influence on the acquired spectra. Phyllosilicates are known to produce characteristic RBs between 8 and 14 μm, often exhibiting a dominant band at ≈10 μm (Michalski et al., 2006; Glotch et al., 2007). Although phyllosilicates in CI chondrites are composed of saponite and serpentine (Tomeoka and Buseck, 1988), the terrestrial reference spectra from the RELAB database diverge from the obtained spectra (Fig. 9). The reflectance maximum of the terrestrial phyllosilicates is shifted towards shorter wavelengths, and the Reststrahlen band shape is different. Beck et al. (2010) have already recognized that terrestrial phyllosilicates are poor analogues for CI and CM chondrites. The exact cause for this observation is not well-constrained. However, it is potentially related to the absence of the crystallographic long-range order in crystalline species within the CI matrix, which leads to optical excitation of certain vibrational modes (Beck et al., 2010). Disordered and amorphous silicate phases are known to show unstructured band peaking ~10 μm (Beck et al., 2010). The comparison of the 10 μm region with synthetic

serpentine does not appear to be a perfect match for the investigated CI spectra. However, band positions of minerals in the MIR are sensitive even to small changes in their chemical composition, so that a varying Mg/Fe ratio, for example in solid solutions, can already shift the position of the Reststrahlenband. Taking further into account that laboratory measurement conditions are hardly ever reproduced identically, may explain the seeming "mismatch" between the database mineral and 'fresh' measurements. Furthermore, terrestrial or synthetic phyllosilicate minerals in the form of endmembers likely have not experienced alteration pathways that their extra-terrestrial counterparts have underwent (e.g, SW). So that a direct comparison with database minerals is possible only with caution and emphasizes the importance of dedicated fitting procedures and analogue materials.

The mineralogy of CI chondrites is dominated by a fine-grained phyllosilicate-bearing matrix, which makes up 94 vol% on average (Alfing et al., 2019). Yet, all investigated lithologies contain a certain admixture of minor constituents. Even if a "pure matrix" spectrum is acquired, sub-micrometer sized grains of minerals like magnetite or pyrrhotite are present. Typical minor constituents include magnetite (4.3 vol%), pyrrhotite (1.1 vol%), carbonates (0.5 vol%), phosphates (0.05 vol%), and olivine or pyroxene grains (0.06 vol%) (Alfing et al., 2019). Due to the brecciated nature of CI chondrites (e.g., Bischoff, 1998; Morlok et al., 2006a; Alfing et al., 2019), the distribution of these minerals is not homogenous, and local enrichments of a certain mineral are often present. This is especially relevant on a microscopic scale, and raises the question whether a specific mineral contribution, has a detectable impact on the MIR spectrum. Two distinct aspects need to be considered: 1) Does a mineral show diagnostic features in the investigated wavelength region, and 2) the mineral abundance threshold that needs to be exceeded to enable detection in the respective electromagnetic region. Although the comparison with literature or database data should be performed with caution (due to potential differences in measurement settings, sample type/quality), it principally shows where characteristic bands can be expected (Fig. 9).

Magnetite is ubiquitous in CI chondrites, and no measurement area was completely free of magnetite. Work by Glotch and Rossman (2009) implies that magnetite single crystals have no characteristic bands in the investigated wavelength region. The influence of magnetite can therefore not be spectroscopically inferred, as magnetite does not affect the spectrum in this wavelength region. This is further confirmed by our observation that analyses from magnetite-rich regions in Ryugu show no significant deviation from the average Ryugu spectrum.

Sulfides seem to affect the spectrum as seen for Ruygu (Fig. 9), although diagnostic bands are absent. A high sulfide contribution leads to an elevated background and decreased RB intensity. In the OH band region around 3 μm, we observed an increased slope between 2.8 and 3 μm for the sulfide-rich region (Fig. 9a). Additionally, the water band area is decreased and the band center is shifted to shorter wavelengths. Yet, we cannot certainly attribute these observations to the presence of sulfides. In theory, pyrrhotite is known to show graybody behavior in the mid-infrared (Hubbard et al., 2023). Material which exhibits systematic graybody radiation, follows a Planck function with a constant emissivity (<1) (Michelsen et al., 2020). Therefore, a pure pyrrhotite spectrum is devoid of characteristic bands in der MIR region.

Dolomite shows diagnostic bands that are distinguishable from other minerals, having two bands at 6.5 and 11.3 μm. The spectrum obtained in the Ryugu section shows a good match with the dolomite spectrum from the RELAB database. The 11.3 μm band corresponds to bending modes of carbonate ions (Prencipe et al., 2004). The features between 6.4 and 7 μm are related to asymmetrical stretching modes of carbonate ions (Prencipe et al., 2004; Gunasekaran et al., 2006). Although the Ca element map indicates that dolomite is quite homogeneously distributed in the Ryugu section A0008, only one spectrum shows carbonate bands. Therefore, we conclude that a substantial dolomite contribution is needed so that characteristic bands are detectable in the MIR spectrum.

Although anhydrous minerals are rare in C1 materials, they have a spectral impact in the MIR region. Olivine and pyroxene are known to exhibit characteristic bands in the MIR region (Hofmeister, 1997; Lane et al., 2011). Typical olivine bands are found between 10 and 12 μm (Morlok et al., 2006b; Lane et al., 2011; Stojic et al., 2021). The abundance of olivine is clearly visible in the spectrum of DaG 319, having two bands at 11.3 and 12 μm. The band at 11.3 μm is also seen in the C1/2 clast in Sahara 98645.

We obtained spectra from the phosphate-rich region in M5 (cf. Fig. 2), in order to test whether a phosphorous-rich matrix would yield a distinct spectral signal. However, no spectral difference compared to the average Ryugu spectrum was observed. Theoretically, phosphate bands can occur in the MIR region due to P—O vibrational modes (Jastrzębski et al., 2011). Yet, spectral bands attributable to phosphate minerals are likely masked by phyllosilicate Reststrahlen bands, especially as the most prominent band, related to asymmetric stretching P—O vibrations, is located at 9.9 μm (e.g., Jastrzębski et al., 2011). Additionally, the phosphate abundance is in general very minor (0.05 vol%) in CI chondrites (Alfing et al., 2019). A spectral feature genuinely related to phosphates present in the matrix was therefore not detected.

Phyllosilicates are by far the most abundant mineral in the investigated lithologies. This dominance is also reflected in the MIR spectra. Our data suggest that the Mg/Fe ratio of phyllosilicates has a subtle, but systematic effect on the features associated with silicate structure and composition (Fig. 11). The correlation between Mg/Fe ratio and CF/RB applies to all investigated samples. As aqueous alteration progresses, serpentine minerals are enriched in Mg, which is in agreement with findings from previous studies by Zolensky et al. (1993), Howard et al. (2009), and McAdam et al. (2015). The change in the Mg/Fe ratio also affects the bonding cation in the hydroxyl stretching mode (M-OH) (Beck et al., 2010).

4.2. Comparing Ryugu, CI chondrites and volatile-rich clasts

Ryugu shows a large overlap with CI chondrites in terms of MIR spectra, mineralogy, and phyllosilicate chemistry. Ivuna and Orgueil show a more pronounced shoulder of the RB at 10.8 μm, which is not as evident in the average Ryugu spectrum. The origin of this feature is ambiguous. However, as opposed to Ryugu, Ivuna and Orgueil show signs of aqueous alteration related to their terrestrial exposure (e.g., sulfate-veins, see King et al., 2020) that can hypothetically explain this feature present in Orgueil, and Ivuna, and also the absence of which in the fresh material of Ryugu (for a detailed spectral analysis of sulfate minerals in the NIR/MIR, see e.g., Cloutis et al., 2006). Alternatively, the 10.8 μm feature might be related to an admixture of an unidentified component, or is related to a non-compositional effect, like the aforementioned lack of crystallographic order, or the high sample porosity (on average 41 vol%) observed for Ryugu samples (e.g. Nakamura et al., 2022). Potentially, the splitting of transverse and longitudinal waves of silicates (LO-TO splitting) is linked to the shoulder at 10.8 μm, as this effect is known to occur in the mid infrared region (e.g., Hofmeister, 1987). For instance, fayalite-rich olivine in the B_{2u}-orientation exhibits a prominent band at 10.87 μm attributed to the υ_{LO} vibration (Hofmeister, 1987). The high sample porosity may explain why epoxy-related features are most prominent in the acquired Ryugu spectra, as opposed to Ivuna and Orgueil. The ethanol-diluted epoxy used for sample preparation of the Ryugu section (e.g., Nakashima et al., 2023) infiltrates the pore spaces, and a pore size dependent portion of the analyzed sample area is comprised of epoxy.

Despite spectral and mineralogical similarities, Ryugu samples were found to be free of sulfates and ferrihydrite (Yokoyama et al., 2023; Nakamura et al., 2023), common accessory phases in CI chondrites (e.g., Tomeoka and Buseck, 1988; Zolensky et al., 1993). Additionally, the amount of interlayer water is different (Yokoyama et al., 2023). Most likely, these differences are best explained by terrestrial contamination (Yokoyama et al., 2023; Nakamura et al., 2023). These findings stress that CI-like material is extremely sensitive for contamination, and Ryugu

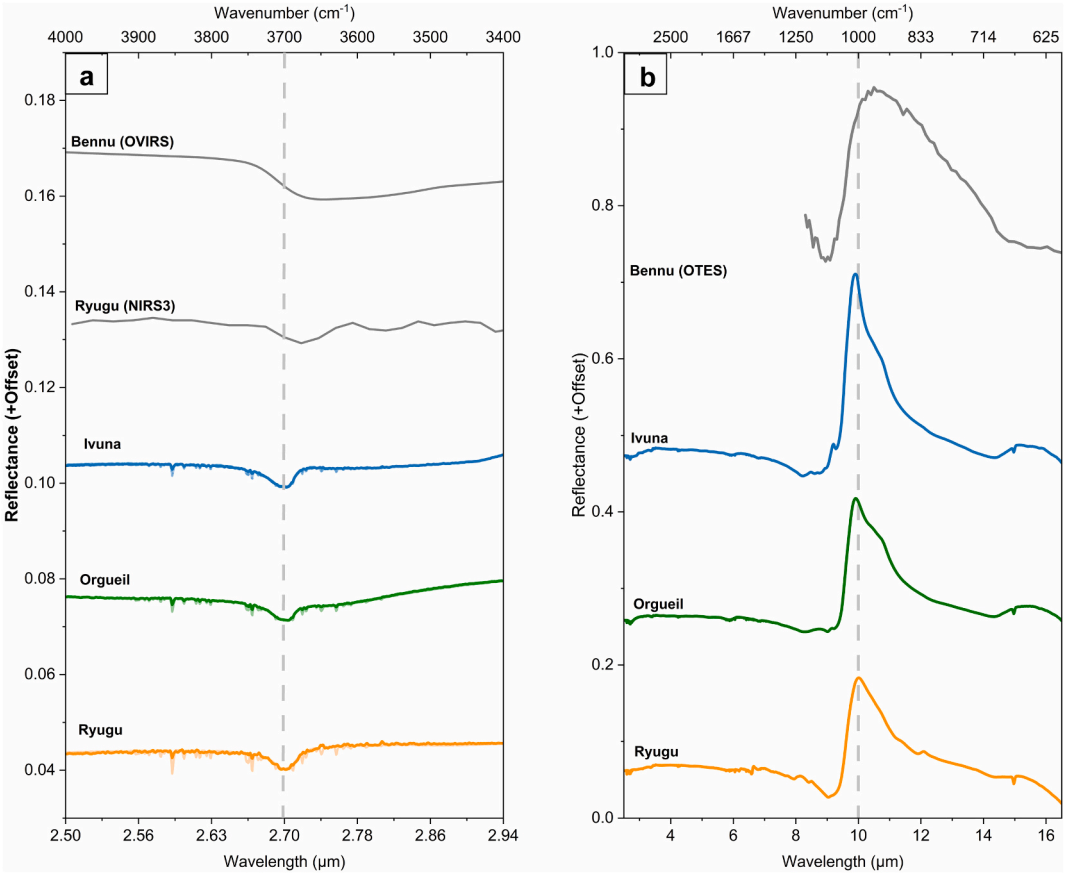

Fig. 7. Comparison of averaged spectra from Ryugu, Ivuna, and Orgueil. Asteroid spectra of Ryugu from Kitazato et al. (2019), and Bennu from Hamilton et al. (2019), Simon et al. (2020), and Nakamura et al. (2023) in grey. The reflectance of asteroid spectra is scaled for better comparison. Dashed lines indicate the (a) typical OH band position (2.7 μm), and (b) Reststrahlen band position (10 μm).

is more pristine than CI chondrites.

The spectra of C1 clasts are largely similar to CI chondrites, and show in principle the same features. On average, the C1/C2 clasts show a more Fe-rich phyllosilicate composition, consistently having Mg/Fe ratios <1, which is spectroscopically reflected in slightly lower CF/RB ratios. Although the position of the OH band is constant (except for the C2 clast in DaG 319), the different nature of the samples (thin sections/thick sections) seems to affect the band intensity (i.e., saturation effects). Therefore, the OH band area of Ryugu, Ivuna, and Orgueil (thick sections) cannot be directly compared to the volatile-rich clasts (thin sections).

The C2 clast in DaG 319 is clearly distinct from the other samples. The clast contains Fe—Ni metal, a TCI, and chondrules, phases that are absent in the investigated C1 clasts. The high abundance of anhydrous minerals (olivine, pyroxene) and metal is related to a lower degree of aqueous alteration. Additionally, the phyllosilicates in the C2 clast are more Fe-rich, which is reflected in even lower CF/RB ratios (Fig. 11a). The spectrum of the clast in DaG 319 shows a less developed water band, and a substantial peak broadening in the 10 μm region, with two additional peaks at 11.3 and 12 μm (Fig. 10). These two are indicative of olivine (Lane et al., 2011). The OH absorption band clearly has a distinct shape, as recorded by the shifted band position and small band area (Table 1). A broad RB band and a shifted band center towards longer wavelength has also been observed for CM chondrites (e.g., Bischoff et al., 2021; Nakamura et al., 2023). Hence the C2 clast is spectrally more similar to CM2 chondrites, and distinguishable from typical CI1 spectra.

The high amount of anhydrous minerals in the clast of Sahara 98,645 indicates that the aqueous alteration is not as progressed as in the other C1 clast investigated. This is also spectrally evident in form of a small band at 11.4 μm, indicative of olivine. Additionally, the OH band is significantly less pronounced compared to the other C1 samples. However, the OH band center is not shifted to longer wavelengths as in the C2 clast, and mineralogically, the C1/2 clast in Sahara 98,645 is also distinct from the C2 clast, as Fe—Ni metal, chondrules, and TCIs are absent.

Although considerable textural variability among the clasts is present, the clasts show less intra-sample heterogeneity compared to CI chondrites (Fig. 5). This might either indicate that the clasts experienced different formation conditions, or alternatively, this observation is primarily related to a sample size effect. As the temperature range and timing of aqueous alteration in C1 clasts coincides with CI chondrites (Visser et al., 2018; Visser et al., 2020), the latter case appears more likely. The textural and mineralogic variability would then be the result of sampling a certain CI-like/C1 lithology, which are breccias themselves. Assuming the secondary processing conditions for C1 clasts were similar as for CI chondrites, chemical and isotopic differences are most likely related to sampling different parent bodies. Although the diversity of C1 parent bodies in the early Solar System is poorly constrained, rare examples are found among ungrouped carbonaceous meteorites such as Flensburg. The ungrouped C1 meteorite Flensburg is the oldest chondrite sample in which contemporaneous episodes of aqueous alteration and brecciation have been preserved (Bischoff et al., 2021). With a CF at 9 μm, and an intense RB at 10 μm, the spectrum of Flensburg is very similar to spectra of Ryugu and CI chondrites. However, mineralogic differences exist especially in regards to the abundance of minor constituents. Carbonates (≈4 vol%) are the second most common constituent after phyllosilicates (≈90 vol%), followed by sulfides (≈3.8 vol%)

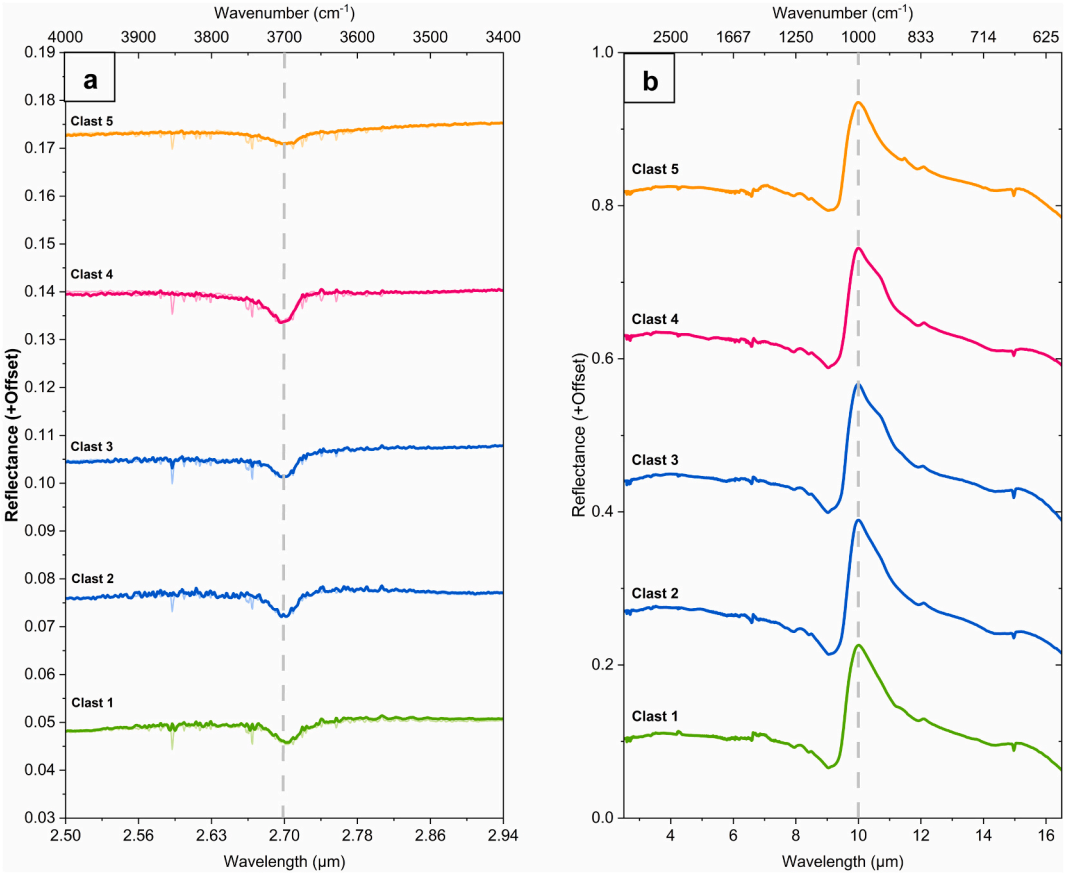

Fig. 8. Spectra from different clasts in Ryugu A0008 (see Fig. 2a). The colors correspond to sites of interest marked in Fig. 2b. Dashed lines indicate the (a) typical OH band position (2.7 μm), and (b) Reststrahlen band position (10 μm).

and magnetite (≈1.9 vol%). Although the MIR spectra of Flensburg and CI chondrites are basically indistinguishable from each other, they are different from spectra of CM, CH and CV chondrites (Bischoff et al., 2021).

In conclusion, aqueous alteration and phyllosilicate chemistry have a major impact on the MIR spectrum. If the spectra are of high quality (i.e., good signal-to-noise ratio and high spectral resolution), MIR spectra can be used to detected even minor differences between carbonaceous samples.

4.3. Linking laboratory spectra with remote sensing data

One key advantage of the MIR region is that it is sensitive to silicate mineralogy. Minerals like olivine, pyroxene, and feldspars are known to produce diagnostic features in this spectral range (e.g., Hofmeister, 1997; Lane et al., 2011; Reitze et al., 2020; Reitze et al., 2021; Stojic et al., 2021). However, MIR spectra are also affected by non-compositional effects such as grain size, porosity, phase angle, temperature, and ambient pressure (e.g., Logan et al., 1973; Reddy et al., 2015).

Kitazato et al. (2019) reported that in the NIR spectra of asteroid Ryugu the most prominent feature is an absorption band at 2.72 μm, associated with Mg-rich phyllosilicates. This feature appears to be constant across Ryugu's surface, indicating a homogeneous composition of the asteroid's surface. The absorption band at 3 μm has been intensively studied and attributed to hydrated silicate minerals (Salisbury et al., 1991; Miyamoto and Zolensky, 1994). It has also been considered in asteroid classification, where it is commonly associated with C-type asteroids (Jones et al., 1990; Lebofsky et al., 1990). The OH absorption band obtained by the NIRS3 instrument (Kitazato et al., 2019) is in good agreement with the spectra of Ryugu A0008 obtained in the laboratory (Fig. 7). Compared to the laboratory spectrum, the NIRS3 spectrum shows a worse signal-to-noise ratio, and a slightly shifted band center towards longer wavelengths. Since the OH absorption feature is not as pronounced as in CI chondrites, it was suggested that Ryugu consists of CI-like or CM-like material which has been thermally altered (Kitazato et al., 2019). However, the difference in band depth between remote sensing and laboratory spectra could be related to space weathering, which is known to affect the OH band at 2.7 μm (e.g., Lantz et al., 2017; Kitazato et al., 2019; Noguchi et al., 2023). Space-exposed surfaces are affected by amorphization and partial melting of phyllosilicates, leading to reduction from Fe^{3+} to Fe^{2+} and dehydration, resulting in a weakening of the OH band (Noguchi et al., 2023). To remove most of the outer space weathering affected layer of Ryugu, an artificial impact crater was produced at the second touchdown site before sample extraction (Saiki et al., 2017; Arakawa et al., 2017, 2020; Nakamura et al., 2022). These samples can be considered more pristine compared to the outermost surface layer of Ryugu. It was shown that excavated material from Ryugu's subsurface has a stronger and peak-shifted OH absorption feature when compared to reflectance spectra of the surface (Kitazato et al., 2021). The peak shift of the 2.7 μm absorption band has been related to space weathering effects, altering Ryugu's surface layer (Hiroi et al., 2023). Another aspect worth mentioning is that the absolute band depth of the absorption feature at 2.7 μm is also depending on the thermal correction of the remote sensing spectra (Kitazato et al., 2019). The here obtained Ryugu spectra show an overwhelming match with CI chondrites. In accordance with these findings, the first laboratory studies of Ryugu samples came to the conclusion that Ryugu was most likely never heated above 100 °C (Yokoyama et al., 2023).

A study by Hamm et al. (2022) compared the MIR emissivity of Ryugu obtained by the MARA infrared radiometer to reflectance spectra

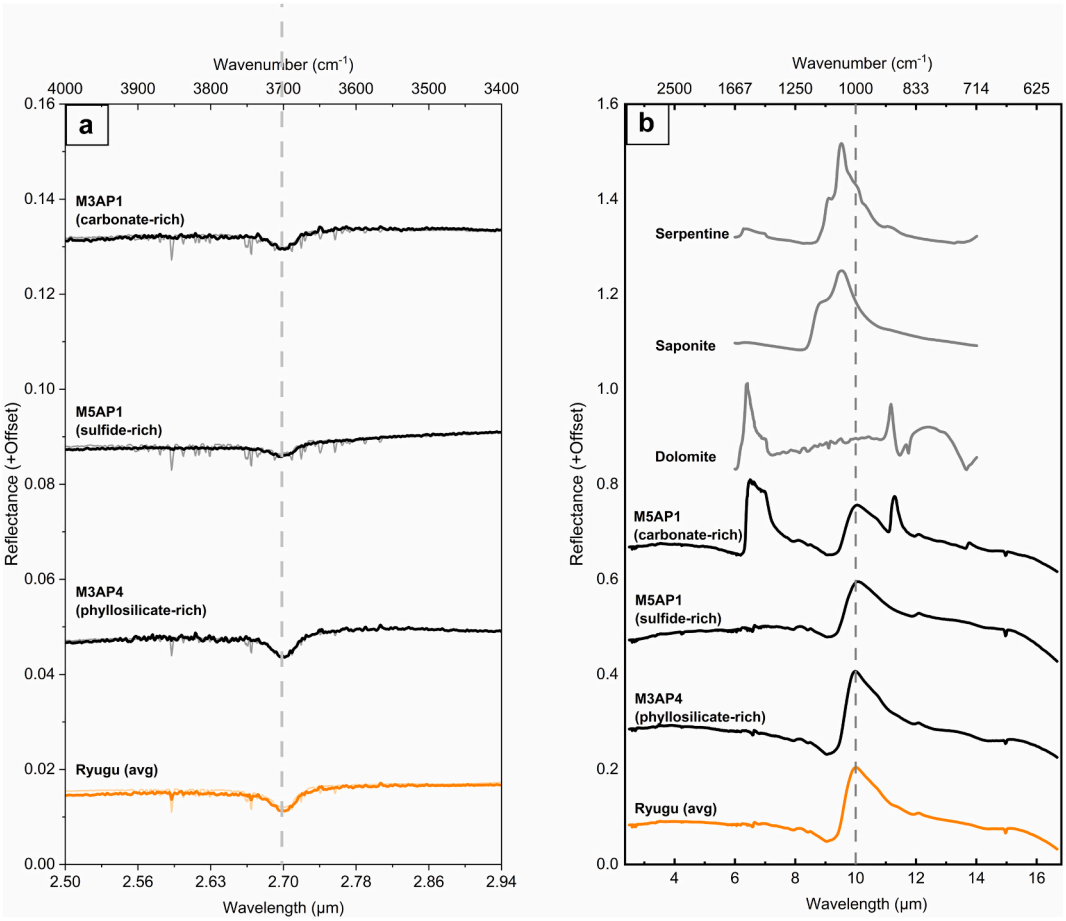

Fig. 9. Ryugu average spectrum (orange) compared to single spectra from different sites of interest enriched in a specific mineral. Mineral spectra in grey are taken from the RELAB database for reference. Dashed lines indicate the (a) typical OH band position (2.7 μm), and (b) Reststrahlen band position (10 μm).

of thin sections of various carbonaceous chondrites. In principle, emissivity spectra obtained by remote sensing can be converted to reflectance spectra by using Kirchhoff's law (e.g., Nicodemus, 1965). Although the spectral contrast of inverted reflectance spectra can be different from emissivity spectra, the position and shape of bands is comparable (e.g., Henderson and Jakosky, 1994; Henderson and Jakosky, 1997; Byrnes et al., 2007; Lee et al., 2010; Morlok et al., 2017). Hamm et al. (2022) concluded that thin sections of CI chondrites provided a better match for the remotely acquired spectra of Ryugu compared to powdered samples. The authors attribute this to Ryugu not being dominated by dust and regolith, but rather by highly porous boulders. In fine-grained powdered samples, the emissivity is a combination of Si—O bond vibrations and transparency features caused by volume scattering effects. Grain size effects are known to decrease the intensity of the RBs inversely proportional to particle size (Salisbury et al., 1987; Reddy et al., 2015), and with smaller particle sizes, transparency features (TF) related to volume scattering become more dominant (Le Bras and Erard, 2003). The TF typically emerges in powdered samples with particle sizes <50–75 μm (Salisbury and Wald, 1992; Salisbury et al., 1997; Le Bras and Erard, 2003). However, it is absent in amorphous samples, e.g., space weathered or impacted materials (Moroz et al., 2009, Palomba et al., 2019), and is also missing in thin sections, where the emissivity maximum is representative of fundamental Si—O vibrations (Hamm et al., 2022). The spectral link of Ryugu and CI chondrites has been spectrally confirmed by recent studies (Nakamura et al., 2023; Dartois et al., 2023).

If compositional information is derived from spectra, also non-compositional effects should be considered. This includes temperature, pressure, phase angle, and grain size effects. Depending on the material analyzed in the laboratory, different scattering behavior occurs. Multiple scattering between particles and crystal orientation effects can lead to differences in reflectance spectra of different materials (e.g., powders of different size fractions, single crystals, polished sections). Ideally, the surface properties of the target object are well constrained, so that an adequate analogue is used, compensating for several non-compositional effects. Additionally, secondary processes causing compositional and physical changes, e.g., space weathering, have to be considered when comparing remote sensing data with laboratory samples.

Although the spectral differences are subtle, our findings indicate that C1 and C2 clasts can be distinguished from CI chondrites within a laboratory framework. Presumably, intra-sample heterogeneity seen on a microscopic scale does not have a prominent effect at the spatial scale conventionally used in remote sensing. The practically more relevant aspects for comparison of in situ acquired micro-FTIR spectra and remote sensing spectra are 1) the quality and spectral resolution of the obtained spectra, and 2) the influence of non-compositional effects. The first aspect is strongly bound to the technological progress of the analytical instrument used in space missions. The second aspect can be addressed by using appropriate analogues, imitating the surface properties of asteroid surfaces. Spectral databases such as the MERTIS Infrared and Raman for Interplanetary Spectroscopy (IRIS) database (Hiesinger et al., 2020), can significantly help to interpret data acquired by remote sensing by providing the basis for spectral deconvolution. Well characterized materials from sample return missions like Hayabusa2 and OSIRIS-REx, allow to establish robust spectral endmembers, which can help to reduce the ambiguity of meteorite-asteroid links. Our study indicates that under ideal conditions, subtle differences among hydrated CC materials can be spectrally identified.

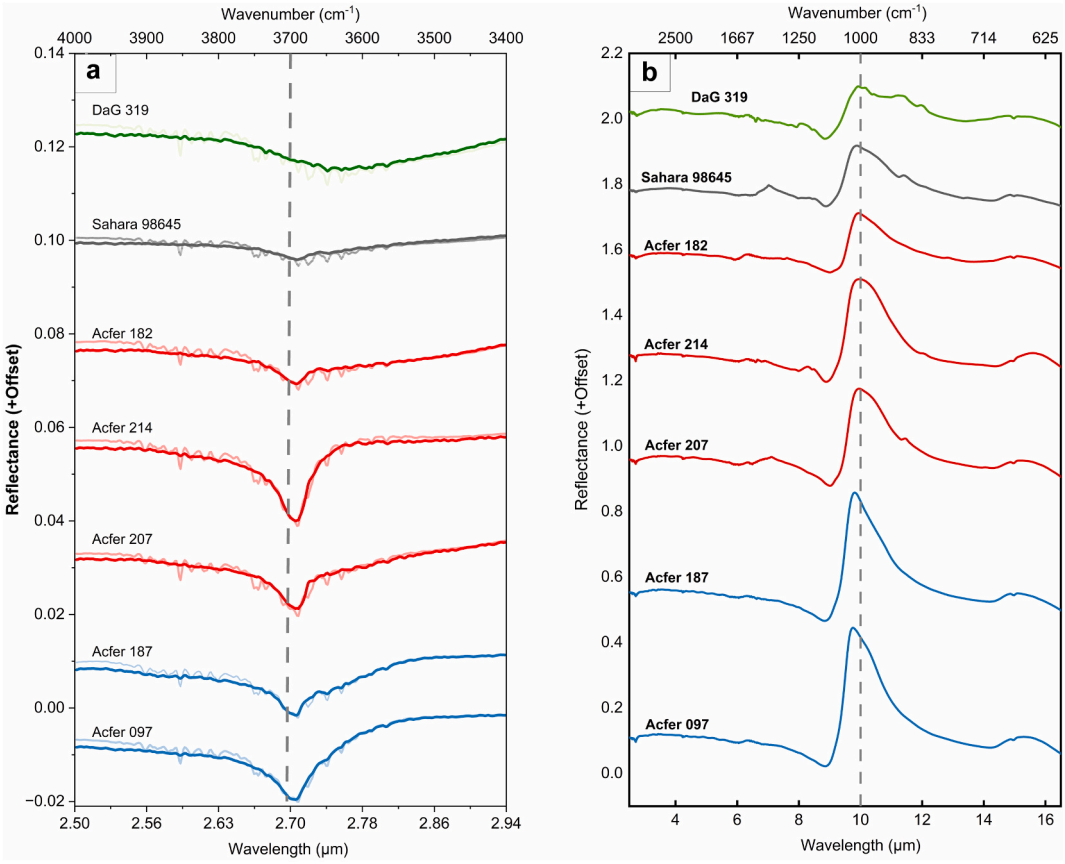

Fig. 10. Averaged spectra of C1 and C2 clasts. Blue = CR, red = CH, grey = OC, green = Ureilite. Dashed lines indicate the (a) typical OH band position (2.7 μm), and (b) Reststrahlen band position (10 μm). (For interpretation of the references to colour in this figure legend, the reader is referred to the web version of this article.)

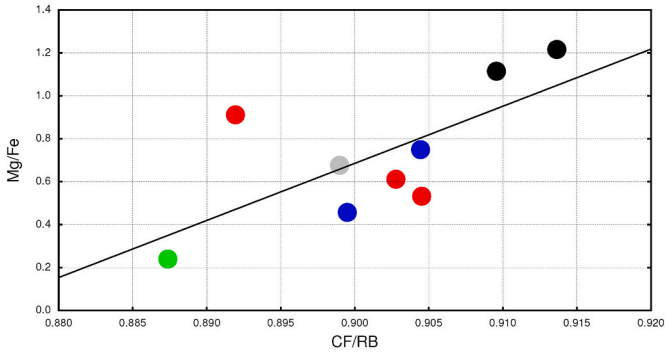

Fig. 11. Correlation between phyllosilicate composition (Mg/Fe ratio) and CF/RB band position ratio (PC of linear fit 0.46). Colors indicate host meteorites: Blue = CR, red = CH, grey = OC, green = Ureilite. (For interpretation of the references to colour in this figure legend, the reader is referred to the web version of this article.)

5. Conclusion

If analytical artifacts are removed and spectral data are processed in a consistent manner, MIR reflectance spectra can be used to investigate meteorite-asteroid links. The main findings can be summarized as following:

1) Except for the C2 clast, all investigated samples show similar features having a discernable OH absorption band at 2.7 μm, the CF at ~9 μm, and a pronounced Reststrahlen band at ~10 μm.
2) The Ruygu sample A0008 shows a brecciated texture, but is spectrally relatively homogeneous. Among the investigated samples, Ryugu sample A0008 is spectrally and petrographically most similar to Orgueil.
3) The average phyllosilicate composition of C1 and C2 clasts is more Fe-rich compared to bulk CI chondrites, which is spectroscopically reflected in lower CF/RB ratios. The investigated samples show a weakly linear correlation of the Mg/Fe ratio in phyllosilicates and the CF/RB band position.
4) The C2 clast in DaG 319 is spectroscopically distinguishable from the other samples, due to differences in mineralogy related to a lower degree of aqueous alteration. This includes a shifted and less developed OH absorption band, and a broad Reststrahlen band (RB) at 10 μm, with two minor RBs emerging at 11.3 and 12 μm.
5) If a certain modal abundance is reached, minor constituents like dolomite and pyrrhotite can affect the spectrum. This is especially relevant on a microscopic scale, as Ryugu and CI chondrites are breccias, and can contain lithologies enriched in a specific mineral. However, other minerals like magnetite have no apparent effect in the investigated wavelength region.
6) Considering Ryugu, the spectra obtained by μ-FTIR on sample A0008 can be compared to remote sensing data on a qualitative level. This demonstrates that micro-FTIR is a powerful tool to characterize intra-sample heterogeneity and very small samples (< 3 mm).

CRediT authorship contribution statement

J. Storz: Writing – review & editing, Writing – original draft, Visualization, Methodology, Investigation, Formal analysis, Conceptualization. **M.P. Reitze:** Writing – review & editing, Methodology, Investigation. **A.N. Stojic:** Writing – review & editing, Methodology,

Investigation. **I. Kerraouch:** Writing – review & editing, Investigation. **A. Bischoff:** Writing – review & editing, Supervision, Project administration, Funding acquisition. **H. Hiesinger:** Project administration, Funding acquisition. **T. John:** Writing – review & editing, Supervision, Project administration, Funding acquisition.

Declaration of competing interest

The authors declare that they have no known competing financial interests or personal relationships that could have appeared to influence the work reported in this paper.

Data availability

Data will be made available on request.

Acknowledgements

We want to thank two anonymous reviewers, who helped to improve the quality of this manuscript greatly. We also thank Andreas Morlok, Ottaviano Rüsch and Markus Patzek for the helpful feedback and their suggestions. We also thank Ulla Heitmann for sample preparation. Hayabusa2 is a mission by the Japanese Aerospace Exploration Agency (JAXA). We want to thank JAXA for providing the Ryugu sample, and Daisuke Nakashima from the Tohoku University for preparing the sample. We thank T. Nakamura and his team for their support of the project. We also thank the staff of the NASA Reflectance Experiment Laboratory (RELAB) for maintaining the spectral database, and all cited researchers who made their data available. M.P. Reitze and A.N. Stojic are supported by the DLR funding 50 QW 2201A in the framework of the BepiColombo mission. This work is funded by the Deutsche Forschungsgemeinschaft (DFG, German Research Foundation) – Project-ID 263649064 – TRR 170. This is TRR 170 Publication No. 205.

Appendix A. Supplementary data

Supplementary data to this article can be found online at https://doi.org/10.1016/j.icarus.2024.116189.

References

Alfing, J., Patzek, M., Bischoff, A., 2019. Modal abundances of coarse-grained (>5 μm) components within CI-chondrites and their individual clasts – Mixing of various lithologies on the CI parent body(ies). Geochemistry 79, 125532.

Arakawa, M., Wada, K., Saiki, T., et al., 2017. Scientific objectives of small carry-on impactor (SCI) and deployable camera 3 digital (DCAM3-D): observation of an ejecta curtain and a crater formed on the surface of Ryugu by an artificial high-velocity impact. Space Sci. Rev. 208, 187–212.

Arakawa, M., et al., 2020. An artificial impact on the asteroid (162173) Ryugu formed a crater in the gravity-dominated regime. Science 368, 67–71.

Bates, H.C., King, A.J., Donaldson, Hanna K.L., Bowles, N.E., Russell, S.S., 2020. Linking mineralogy and spectroscopy of highly aqueously altered CM and CI carbonaceous chondrites in preparation for primitive asteroid sample return. MAPS 55, 77–101.

Beck, P., Quirico, E., Montes-Hernandez, G., Bonal, L., Bollard, J., Orthous-Daunay, F.-R., Howard, K.T., Schmitt, B., Brissaud, O., Deschamps, F., Wunder, B., Guillot, S., 2010. Hydrous mineralogy of CM and CI chondrites from infrared spectroscopy and their relationship with low albedo asteroids. GCA 74, 4881–4892.

Beck, P., Garenne, A., Quirico, E., Bonal, L., Montes-Hernandez, G., Moynier, F., Schmitt, B., 2014. Transmission infrared spectra (2–25μm) of carbonaceous chondrites (CI, CM, CV–CK, CR, C2 ungrouped): mineralogy, water, and asteroidal processes. Icarus 229, 263–277.

Bischoff, A., 1998. Aqueous alteration of carbonaceous chondrites: evidence for preaccretionary alteration-A review. MAPS 33, 1113–1122.

Bischoff, A., Palme, H., Schultz, L., Weber, D., Weber, H.W., Spettel, B., 1993a. Acfer 182 and paired samples, an iron-rich carbonaceous chondrite: similarities with ALH85085 and relationship to CR chondrites. GCA 57, 2631–2648.

Bischoff, A., Palme, H., Ash, R.D., Clayton, R.N., Schultz, L., Herpers, U., Stöffler, D., Grady, M.M., Pillinger, C.T., Spettel, B., Weber, H., Grund, T., Endreβ, M., Weber, D., 1993b. Paired Renazzo-type (CR) carbonaceous chondrites from the Sahara. GCA 57, 1587–1603.

Bischoff, A., Schleiting, M., Wieler, R., Patzek, M., 2018. Brecciation among 2280 ordinary chondrites – constraints on the evolution of their parent bodies. GCA 238, 516–541.

Bischoff, A., Alexander, C.M.O., Barrat, J.-A., Burkhardt, C., Busemann, H., Degering, D., Di Rocco, T., Fischer, M., Fockenberg, T., Foustoukos, D.I., Gattacceca, J., Godinho, J.R., Harries, D., Heinlein, D., Hellmann, J.L., Hertkorn, N., Holm, A., Jull, A.T., Kerraouch, I., King, A.J., Kleine, T., Koll, D., Lachner, J., Ludwig, T., Merchel, S., Mertens, C.A., Morino, P., Neumann, W., Pack, A., Patzek, M., Pavetich, S., Reitze, M.P., Rüfenacht, M., Rugel, G., Schmidt, C., Schmitt-Kopplin, P., Schönbächler, M., Trieloff, M., Wallner, A., Wimmer, K., Wölfer, E., 2021. The old, unique C1 chondrite Flensburg – insight into the first processes of aqueous alteration, brecciation, and the diversity of water-bearing parent bodies and lithologies. GCA 293, 142–186.

Braukmüller, N., Wombacher, F., Funk, C., Münker, C., 2019. Earth's volatile element depletion pattern inherited from a carbonaceous chondrite-like source. Nat. Geosci. 12, 564–568.

Brearley, A.J., McSween, H.Y., 2006. The action of water. In: Walker, R.M., Cameron, A. G.W., Lauretta, D.S. (Eds.), Meteorites and the Early Solar System II. University of Arizona Press, pp. 584–624.

Briani, G., Gounelle, M., Bourot-Denise, M., Zolensky, M.E., 2012. Xenoliths and microxenoliths in H chondrites: sampling the zodiacal cloud in the asteroid Main Belt. MAPS 47, 880–902.

Bus, S., Binzel, R.P., 2002. Phase II of the small main-belt asteroid spectroscopic survey: A feature-based taxonomy. Icarus 158, 146–177.

Byrnes, J.M., Ramsey, M.S., King, P.L., Lee, R.J., 2007. Thermal infrared reflectance and emission spectroscopy of Quartz-Feldspathic glasses. Geophys. Res. Lett. 34.

Cloutis, E.A., Hawthorne, F.C., Mertzman, S.A., Krenn, K., Craig, M.A., Marcino, D., Methot, M., Strong, J., Mustard, J.F., Blaney, D.L., Bell III, J.F., Vilas, F., 2006. Detection and discrimination of sulfate minerals using reflectance spectroscopy. Icarus 184 (1), 121–157.

Conel, J.E., 1969. Infrared emissivities of silicates: experimental results and a cloudy atmosphere model of spectral emission from condensed particulate mediums. J. Geophys. Res. 74, 1614–1634.

Dartois, E., Kebukawa, Y., Yabuta, H., Mathurin, J., Engrand, C., Duprat, J., Bejach, L., Dazzi, A., Deniset-Besseau, A., Bonal, L., Quirico, E., Sandt, C., Borondics, F., Barosch, J., Cody, G., De Gregorio, B., Hashiguchi, M., Kilcoyne, D., Komatsu, M., Martins, Z., Matsumoto, M., Montagnac, G., Mostefaoui, S., Nittler, L., Ohigashi, T., Okumura, T., Remusat, L., Sandford, S., Shigenaka, M., Stroud, R., Suga, H., Takahashi, Y., Takeichi, Y., Tamenori, Y., Verdier-Paoletti, M., Yamashita, S., Nakamura, T., Morita, T., Kikuiri, M., Amano, K., Kagawa, E., Noguchi, T., Naraoka, H., Okazaki, R., Sakamoto, K., Yurimoto, H., Abe, M., Kamide, K., Miyazaki, A., Nakato, A., Nakazawa, S., Nishimura, M., Okada, T., Saiki, T., Tachibana, S., Tanaka, S., Terui, F., Tsuda, Y., Usui, T., Watanabe, S., Yada, T., Yogata, K., Yoshikawa, M., 2023. Chemical composition of carbonaceous asteroid Ryugu from synchrotron spectroscopy in the mid- to far-infrared of Hayabusa2-returned samples. A&A 671.

DeMeo, F.E., Carry, B., 2013. The taxonomic distribution of asteroids from multi-filter all-sky photometric surveys. Icarus 226, 723–741.

DeMeo, F.E., Binzel, R.P., Slivan, S.M., Bus, S.J., 2009. An extension of the Bus asteroid taxonomy into the near-infrared. Icarus 202, 160–180.

DeMeo, F.E., Burt, B.J., Marsset, M., Polishook, D., Burbine, T.H., Carry, B., Binzel, R.P., Vernazza, P., Reddy, V., Tang, M., Thomas, C.A., Rivkin, A.S., Moskovitz, N.A., Slivan, S.M., Bus, S.J., 2022. Connecting asteroids and meteorites with visible and near-infrared spectroscopy. Icarus 380, 114971.

Emery, J.P., Cruikshank, D.P., van Cleve, J., 2006. Thermal emission spectroscopy (5.2–38 μm) of three Trojan asteroids with the Spitzer space telescope: detection of fine-grained silicates. Icarus 182, 496–512.

Endreß, M., Keil, K., Bischoff, A., Spettel, B., Clayton, R.N., Mayeda, T.K., 1994. Origin of dark clasts in the Acfer 059/El Djouf 001 CR2 chondrite. Meteoritics 29, 26–40.

Gaffey, M.J., Burbine, T.H., Binzel, R.P., 1993. Asteroid spectroscopy: Progress and perspectives. MAPSs 28, 161–187.

Glotch, T.D., Rossman, G.R., 2009. Mid-infrared reflectance spectra and optical constants of six iron oxide/oxyhydroxide phases. Icarus 204, 663–671.

Glotch, T.D., Rossman, G.R., Aharonson, O., 2007. Mid-infrared (5–100 μm) reflectance spectra and optical constants of ten phyllosilicate minerals. Icarus 192, 605–622.

Goodrich, C.A., Zolensky, M.E., Fioretti, A.M., Shaddad, M.H., Downes, H., Hiroi, T., Kohl, I., Young, E.D., Kita, N.T., Hamilton, V.E., Riebe, M.E.I., Busemann, H., Macke, R.J., Fries, M., Ross, D.K., Jenniskens, P., 2019. The first samples from Almahata Sitta showing contacts between Ureilitic and chondritic Lithologies: implications for the structure and composition of asteroid 2008 TC3. Meteorit. Planet. Sci. 54, 2769–2813.

Greenwood, R.C., Franchi, I.A., Findlay, R., Malley, J.A., Ito, M., Yamaguchi, A., Kimura, M., Tomioka, N., Uesugi, M., Imae, N., Shirai, N., Ohigashi, T., Liu, M.-C., McCain, K.A., Matsuda, N., McKeegan, K.D., Uesugi, K., Nakato, A., Yogata, K., Yuzawa, H., Kodama, Y., Tsuchiyama, A., Yasutake, M., Hirahara, K., Tekeuchi, A., Sekimoto, S., Sakurai, I., Okada, I., Karouji, Y., Nakazawa, S., Okada, T., Saiki, T., Tanaka, S., Terui, F., Yoshikawa, M., Miyazaki, A., Nishimura, M., Yada, T., Abe, M., Usui, T., Watanabe, S., Tsuda, Y., 2023. Oxygen isotope evidence from Ryugu samples for early water delivery to Earth by CI chondrites. Nat. Astronomy 7, 29–38.

Grott, M., Biele, J., Michel, P., Sugita, S., Schröder, S., Sakatani, N., Neumann, W., Kameda, S., Michikami, T., Honda, C., 2020. Macroporosity and grain density of rubble pile asteroid (162173) Ryugu. J. Geophys. Res. Planets 125.

Gunasekaran, S., Anbalagan, G., Pandi, S., 2006. Raman and infrared spectra of carbonates of calcite structure. J. Raman Spectrosc. 37, 892–899.

Hamilton, V.E., Simon, A.A., Christensen, P.R., Reuter, D.C., Clark, B.E., Barucci, M.A., Bowles, N.E., Boynton, W.V., Brucato, J.R., Cloutis, E.A., Connolly, H.C., Hanna, K.L. D., Emery, J.P., Enos, H.L., Fornasier, S., Haberle, C.W., Hanna, R.D., Howell, E.S., Kaplan, H.H., Keller, L.P., Lantz, C., Li, J.-Y., Lim, L.F., McCoy, T.J., Merlin, F., Nolan, M.C., Praet, A., Rozitis, B., Sandford, S.A., Schrader, D.L., Thomas, C.A.,

Zou, X.-D., Lauretta, D.S., 2019. Evidence for widespread hydrated minerals on asteroid (101955) Bennu. Nat. Astron. 3, 332–340.
Hamm, M., Grott, M., Senshu, H., Knollenberg, J., Wiljes, J. de, Hamilton, V.E., Scholten, F., Matz, K.D., Bates, H., Maturilli, A., Shimaki, Y., Sakatani, N., Neumann, W., Okada, T., Preusker, F., Elgner, S., Helbert, J., Kührt, E., Ho, T.-M., Tanaka, S., Jaumann, R., Sugita, S., 2022. Mid-infrared emissivity of partially dehydrated asteroid (162173) Ryugu shows strong signs of aqueous alteration. Nature 13, 364.
Henderson, B.G., Jakosky, B.M., 1994. Near-surface thermal gradients and their effects on mid-infrared emission spectra of planetary surfaces. J. Geophys. Res. 99, 19063–19073.
Henderson, B.G., Jakosky, B.M., 1997. Near-surface thermal gradients and mid-IR emission spectra: A new model including scattering and application to real data. J. Geophys. Res. 102 (E3), 6567–6580.
Hiesinger, H., Helbert, J., Alemanno, G., Bauch, K.E., D'Amore, M., Maturilli, A., Morlok, A., Reitze, M.P., Stangarone, C., Stojic, A.N., Varatharajan, I., Weber, I., 2020. Studying the composition and mineralogy of the Hermean surface with the mercury radiometer and thermal infrared spectrometer (MERTIS) for the BepiColombo mission: an update. Space Sci. Rev. 216.
Hiroi, T., Kaiden, H., Imae, N., Misawa, K., Kojima, H., Sasaki, S., Matsuoka, M., Nakamura, T., Bish, D.L., Ohtsuka, K., Howard, K.T., Robertson, K.R., Milliken, R.E., 2021. UV-visible-infrared spectral survey of Antarctic carbonaceous chondrite chips. Polar Sci. 29, 100723.
Hiroi, T., Milliken, R.E., Robertson, K.M., Schultz, C.D., Amano, K., Nakamura, T., Yurimoto, H., Noguchi, T., Okazaki, R., Naraoka, H., Yabuta, H., Sakamoto, K., Yada, T., Nishimura, M., Nakato, A., Miyazaki, A., Yogata, K., Abe, M., Okada, T., Usui, T., Yoshikawa, M., Saiki, T., Tanaka, S., Nakazawa, S., Yokota, Y., Tatsumi, E., Tsuda, Y., Tachibana, S., Fuyuto, T., Watanabe, S., Sasaki, S., Kaiden, H., Kitazato, K., Matsuoka, M., 2023. Evidence of global space weathering by solar wind on asteroid 162173 Ryugu. Icarus 406, 115755.
Hofmeister, A.M., 1987. Single-crystal absorption and reflection infrared spectroscopy of forsterite and fayalite. Phys. Chem. Miner. 14, 499–513.
Hofmeister, A.M., 1997. Infrared reflectance spectra of fayalite, and absorption data from assorted olivines, including pressure and isotope effects. Phys. Chem. Miner. 24, 535–546.
Howard, K.T., Benedix, G.K., Bland, P.A., Cressey, G., 2009. Modal mineralogy of CM2 chondrites by X-ray diffraction (PSD-XRD). Part 1: Total phyllosilicate abundance and the degree of aqueous alteration. Geochim. Cosmochim. Acta 73, 4576–4589.
Hubbard, K.M., Haberle, C.W., Elkins-Tanton, L.T., Christensen, P.R., Semken, S., 2023. Thermal-infrared emission spectroscopy of Graybody minerals (sulfide): implications for extraterrestrial exploration for magmatic ore deposits. Earth Space Sci. 10.
Jastrzębski, W., Sitarz, M., Rokita, M., Bułat, K., 2011. Infrared spectroscopy of different phosphates structures. Spectrochimica Acta Part A, Molecular and Biomolecular Spectroscopy 79, 722–727.
Jones, T.D., Lebofsky, L.A., Lewis, J.S., Marley, M.S., 1990. The composition and origin of the C, P, and D asteroids: water as a tracer of thermal evolution in the outer belt. Icarus 88, 172–192.
Kerraouch, I., Kebukawa, Y., Bischoff, A., Zolensky, M.E., Wölfer, E., Hellmann, J.L., Ito, M., King, A., Trieloff, M., Barrat, J.-A., Schmitt-Kopplin, P., Pack, A., Patzek, M., Hanna, R.D., Fockenberg, T., Marrocchi, Y., Fries, M., Mathurin, J., Dartois, E., Duprat, J., Engrand, C., Deniset, A., Dazzi, A., Kiryu, K., Igisu, M., Shibuya, T., Wakabayashi, D., Yamashita, S., Takeichi, Y., Takahashi, Y., Ohigashi, T., Kodama, Y., Kondo, M., 2022. Heterogeneous nature of the carbonaceous chondrite breccia Aguas Zarcas – Cosmochemical characterization and origin of new carbonaceous chondrite lithologies. GCA 334, 155–186.
King, A.J., Solomon, J.R., Schofield, P.F., Russell, S.S., 2015. Characterizing the CI and CI-like carbonaceous chondrites using thermogravimetric analysis and infrared spectroscopy. Earth Planet Sp. 67.
King, A.J., Phillips, K.J.H., Strekopytov, S., Vita-Finzi, C., Russell, S.S., 2020. Terrestrial modification of the Ivuna meteorite and a reassessment of the chemical composition of the CI type specimen. GCA 268, 73–89.
Kitazato, K., Milliken, R.E., Iwata, T., Abe, M., Ohtake, M., Matsuura, S., Arai, T., Nakauchi, Y., Nakamura, T., Matsuoka, M., Senshu, H., Hirata, N., Hiroi, T., Pilorget, C., Brunetto, R., Poulet, F., Riu, L., Bibring, J.-P., Takir, D., Domingue, D.L., Vilas, F., Barucci, M.A., Perna, D., Palomba, E., Galiano, A., Tsumura, K., Osawa, T., Komatsu, M., Nakato, A., Takato, N., Matsunaga, T., Takagi, Y., Matsumoto, K., Kouyama, T., Yokota, Y., Tatsumi, E., Sakatani, N., Yamamoto, Y., Okada, T., Sugita, S., Honda, R., Morota, T., Kameda, S., Sawada, H., Honda, C., Yamada, M., Suzuki, H., Yoshioka, K., Hayakawa, M., Ogawa, K., Cho, Y., Shirai, K., Shimaki, Y., Yamaguchi, A., Ogawa, N., Terui, F., Yamaguchi, T., Takei, Y., Saiki, T., Nakazawa, S., Tanaka, S., Yoshikawa, M., Watanabe, S., Tsuda, Y., 2019. The surface composition of asteroid 162173 Ryugu from Hayabusa2 near-infrared spectroscopy. Science 364, 272–275.
Kitazato, K., Milliken, R.E., Iwata, T., et al., 2021. Thermally altered subsurface material of asteroid (162173). Nat. Astron. 5, 246–250.
Lane, M.D., Christensen, P.R., 1997. Thermal infrared emission spectroscopy of anhydrous carbonates. J. Geophys. Res. Planets 102, 25581–25592.
Lane, M.D., Glotch, T.D., Dyar, M.D., Pieters, C.M., Klima, R., Hiroi, T., Bishop, J.L., Sunshine, J., 2011. Midinfrared spectroscopy of synthetic olivines: thermal emission, specular and diffuse reflectance, and attenuated total reflectance studies of forsterite to fayalite. J. Geophys. Res. 116.
Lantz, C., Brunetto, R., Barucci, M.A., Fornasier, S., Baklouti, D., Bourçois, J., Godard, M., 2017. Ion irradiation of carbonaceous chondrites: A new view of space weathering on primitive asteroids. Icarus 285, 43–57.
Le Bras, A., Erard, S., 2003. Reflectance spectra of regolith analogs in the mid-infrared: effects of grain size. Planet. Space Sci. 51, 281–294.
Lebofsky, L.A., Jones, T.D., Owensby, P.D., Feierberg, M.A., Consolmagno, G.J., 1990. The nature of Low-Albedo asteroids from 3-μm multi-color photometry. Icarus 83, 16–26.
Lee, R.J., King, P.L., Ramsey, M.S., 2010. Spectral analysis of synthetic quartzofeldspathic glasses using laboratory thermal infrared spectroscopy. J. Geophys. Res. 115.
Lim, L., Mcconnochie, T., Bell III, J., Hayward, T., 2005. Thermal infrared spectra of 29 asteroids: the Cornell mid-infrared asteroid spectroscopy (MIDAS) survey. Icarus 173, 385–408.
Lodders, K., 2003. Solar system abundances and condensation temperatures of the elements. ApJ 591, 1220–1247.
Logan, L.M., Hunt, G.R., Salisbury, J.W., Balsamo, S.R., 1973. Compositional implications of Christiansen frequency maximums for infrared remote sensing applications. J. Geophys. Res. 78, 4983–5003.
Marty, B., Alexander, C.M.O., Raymond, S.N., 2013. Primordial origins of Earth's carbon. Rev. Mineral. Geochem. 75, 149–181.
McAdam, M.M., Sunshine, J.M., Howard, K.T., McCoy, T.M., 2015. Aqueous alteration on asteroids: linking the mineralogy and spectroscopy of CM and CI chondrites. Icarus 245, 320–332.
Michalski, J.R., Kraft, M.D., Sharp, T.G., Williams, L.B., Christensen, P.R., 2006. Emission spectroscopy of clay minerals and evidence for poorly crystalline aluminosilicates on Mars from thermal emission spectrometer data. JGR: Planets 111 (E3).
Michelsen, H.A., Colket, M.B., Bengtsson, P.-E., D'Anna, A., Desgroux, P., Haynes, B.S., Miller, J.H., Nathan, G.J., Pitsch, H., Wang, H., 2020. A review of terminology used to describe soot formation and evolution under combustion and pyrolytic conditions. ACS Nano 14, 12470–12490.
Miyamoto, M., Zolensky, M.E., 1994. Infrared diffuse reflectance spectra of carbonaceous chondrites: amount of hydrous minerals. Meteoritics 29, 849–853.
Morlok, A., Bischoff, A., Stephan, T., Floss, C., Zinner, E., Jessberger, E.K., 2006a. Brecciation and chemical heterogeneities of CI chondrites. Geochim. Cosmochim. Acta 70, 5371–5394.
Morlok, A., Bowey, J., Köhler, M., Grady, M.M., 2006b. FTIR 2-16 micron spectroscopy of micron-sized olivines from primitive meteorites. Meteorit. Planet. Sci. 41, 773–784.
Morlok, A., Klemme, S., Weber, I., Stojic, A., Sohn, M., Hiesinger, H., 2017. IR spectroscopy of synthetic glasses with mercury surface composition: analogs for remote sensing. Icarus 296, 123–138.
Morlok, A., Schiller, B., Weber, I., Daswani, M.M., Stojic, A.N., Reitze, M.P., Gramse, T., Wolters, S.D., Hiesinger, H., Grady, M.M., Helbert, J., 2020. Mid-infrared reflectance spectroscopy of carbonaceous chondrites and calcium–aluminum-rich inclusions. Planet. Space Sci. 193, 105078.
Morota, T., Sugita, S., Cho, Y., Kanamaru, M., Tatsumi, E., Sakatani, N., Honda, R., Hirata, N., Kikuchi, H., Yamada, M., Yokota, Y., Kameda, S., Matsuoka, M., Sawada, H., Honda, C., Kouyama, T., Ogawa, K., Suzuki, H., Yoshioka, K., Hayakawa, M., Hirabayashi, M., Miyamoto, H., Michikami, T., Hiroi, T., Hemmi, R., Barnouin, O.S., Ernst, C.M., Kitazato, K., Nakamura, T., Riu, L., Senshu, H., Kobayashi, H., Sasaki, S., Komatsu, G., Tanabe, N., Fujii, Y., Irie, T., Suemitsu, M., Takaki, N., Sugimoto, C., Yumoto, K., Ishida, M., Kato, H., Moroi, K., Domingue, D., Michel, P., Pilorget, C., Iwata, T., Abe, M., Ohtake, M., Nakauchi, Y., Tsumura, K., Yabuta, H., Ishihara, Y., Noguchi, R., Matsumoto, K., Miura, A., Namiki, N., Tachibana, S., Arakawa, M., Ikeda, H., Wada, K., Mizuno, T., Hirose, C., Hosoda, S., Mori, O., Shimada, T., Soldini, S., Tsukizaki, R., Yano, H., Ozaki, M., Takeuchi, H., Yamamoto, Y., Okada, T., Shimaki, Y., Shirai, K., Iijima, Y., Noda, H., Kikuchi, S., Yamaguchi, T., Ogawa, N., Ono, G., Mimasu, Y., Yoshikawa, K., Takahashi, T., Takei, Y., Fujii, A., Nakazawa, S., Terui, F., Tanaka, S., Yoshikawa, M., Saiki, T., Watanabe, S., Tsuda, Y., 2020. Sample collection from asteroid (162173) Ryugu by Hayabusa2: implications for surface evolution. Science (New York, N.Y.) 368, 654–659.
Moroz, L.V., Basilevsky, A.T., Hiroi, T., Rout, S.S., Baither, D., Van Der Bogert, C.M., Yakovlev, O.I., Fisenko, A.V., Semjonova, L.F., Rusakov, V.S., Khramov, D.A., Zinovieva, N.G., Arnold, G., Pieters, C.M., 2009. Spectral properties of simulated impact glasses produced from Martian soil analogue JSC Mars-1. Icarus 202 (1), 336–353.
Nakamura, E., Kobayashi, K., Tanaka, R., Kunihiro, T., Kitagawa, H., Potiszil, C., Ota, T., Sakaguchi, C., Yamanaka, M., Ratnayake, D.M., Tripathi, H., Kumar, R., Avramescu, M.-L., Tsuchida, H., Yachi, Y., Miura, H., Abe, M., Fukai, R., Furuya, S., Hatakeda, K., Hayashi, T., Hitomi, Y., Kumagai, K., Miyazaki, A., Nakato, A., Nishimura, M., Okada, T., Soejima, H., Sugita, S., Suzuki, A., Usui, T., Yada, T., Yamamoto, D., Yogata, K., Yoshitake, M., Arakawa, M., Fujii, A., Hayakawa, M., Hirata, N., Hirata, N., Honda, R., Honda, C., Hosoda, S., Iijima, Y.-I., Ikeda, H., Ishiguro, M., Ishihara, Y., Iwata, T., Kawahara, K., Kikuchi, S., Kitazato, K., Matsumoto, K., Matsuoka, M., Michikami, T., Mimasu, Y., Miura, A., Morota, T., Nakazawa, S., Namiki, N., Noda, H., Noguchi, R., Ogawa, N., Ogawa, K., Okamoto, C., Ono, G., Ozaki, M., Saiki, T., Sakatani, N., Sawada, H., Senshu, H., Shimaki, Y., Shirai, K., Takei, Y., Takeuchi, H., Tanaka, S., Tatsumi, E., Terui, F., Tsukizaki, R., Wada, K., Yamada, M., Yamada, T., Yamamoto, Y., Yano, H., Yokota, Y., Yoshihara, K., Yoshikawa, M., Yoshikawa, K., Fujimoto, M., Watanabe, S., Tsuda, Y., 2022. On the origin and evolution of the asteroid Ryugu: A comprehensive geochemical perspective. Proc. Jpn. Acad. Ser. B Phys. Biol. Sci. 98, 227–282.
Nakamura, T., Matsumoto, M., Amano, K., Enokido, Y., Zolensky, M.E., Mikouchi, T., Genda, H., Tanaka, S., Zolotov, M.Y., Kurosawa, K., Wakita, S., Hyodo, R., Nagano, H., Nakashima, D., Takahashi, Y., Fujioka, Y., Kikuiri, M., Kagawa, E., Matsuoka, M., Brearley, A.J., Tsuchiyama, A., Uesugi, M., Matsuno, J., Kimura, Y., Sato, M., Milliken, R.E., Tatsumi, E., Sugita, S., Hiroi, T., Kitazato, K., Brownlee, D., Joswiak, D.J., Takahashi, M., Ninomiya, K., Takahashi, T., Osawa, T., Terada, K.,

Brenker, F.E., Tkalcec, B.J., Vincze, L., Brunetto, R., Aléon-Toppani, A., Chan, Q.H. S., Roskosz, M., Viennet, J.-C., Beck, P., Alp, E.E., Michikami, T., Nagaashi, Y., Tsuji, T., Ino, Y., Martinez, J., Han, J., Dolocan, A., Bodnar, R.J., Tanaka, M., Yoshida, H., Sugiyama, K., King, A.J., Fukushi, K., Suga, H., Yamashita, S., Kawai, T., Inoue, K., Nakato, A., Noguchi, T., Vilas, F., Hendrix, A.R., Jaramillo-Correa, C., Domingue, D.L., Dominguez, G., Gainsforth, Z., Engrand, C., Duprat, J., Russell, S.S., Bonato, E., Ma, C., Kawamoto, T., Wada, T., Watanabe, S., Endo, R., Enju, S., Riu, L., Rubino, S., Tack, P., Takeshita, S., Takeichi, Y., Takeuchi, A., Takigawa, A., Takir, D., Tanigaki, T., Taniguchi, A., Tsukamoto, K., Yagi, T., Yamada, S., Yamamoto, K., Yamashita, Y., Yasutake, M., Uesugi, K., Umegaki, I., Chiu, I., Ishizaki, T., Okumura, S., Palomba, E., Pilorget, C., Potin, S.M., Alasli, A., Anada, S., Araki, Y., Sakatani, N., Schultz, C., Sekizawa, O., Sitzman, S.D., Sugiura, K., Sun, M., Dartois, E., Pauw, E. de, Dionnet, Z., Djouadi, Z., Falkenberg, G., Fujita, R., Fukuma, T., Gearba, I.R., Hagiya, K., Hu, M.Y., Kato, T., Kawamura, T., Kimura, M., Kubo, M.K., Langenhorst, F., Lantz, C., Lavina, B., Lindner, M., Zhao, J., Vekemans, B., Baklouti, D., Bazi, B., Borondics, F., Nagasawa, S., Nishiyama, G., Nitta, K., Mathurin, J., Matsumoto, T., Mitsukawa, I., Miura, H., Miyake, A., Miyake, Y., Yurimoto, H., Okazaki, R., Yabuta, H., Naraoka, H., Sakamoto, K., Tachibana, S., Connolly, H.C., Lauretta, D.S., Yoshitake, M., Yoshikawa, M., Yoshikawa, K., Yoshihara, K., Yokota, Y., Yogata, K., Yano, H., Yamamoto, Y., Yamamoto, D., Yamada, M., Yamada, T., Yada, T., Wada, K., Usui, T., Tsukizaki, R., Terui, F., Takeuchi, H., Takei, Y., Iwamae, A., Soejima, H., Shirai, K., Shimaki, Y., Senshu, H., Sawada, H., Saiki, T., Ozaki, M., Ono, G., Okada, T., Ogawa, N., Ogawa, K., Noguchi, R., Noda, H., Nishimura, M., Namiki, N., Nakazawa, S., Morota, T., Miyazaki, A., Miura, A., Mimasu, Y., Matsumoto, K., Kumagai, K., Kouyama, T., Kikuchi, S., Kawahara, K., Kameda, S., Iwata, T., Ishihara, Y., Ishiguro, M., Ikeda, H., Hosoda, S., Honda, R., Honda, C., Hitomi, Y., Hirata, N., Hayashi, T., Hayakawa, M., Hatakeda, K., Furuya, S., Fukai, R., Fujii, A., Cho, Y., Arakawa, M., Abe, M., Tsuda, Y., 2023. Formation and evolution of carbonaceous asteroid Ryugu: direct evidence from returned samples. Science (New York, N.Y.) 379, eabn8671.

Nakashima, D., Fujioka, Y., Katayama, K., Morita, T., Kikuiri, M., Amano, K., Kagawa, E., Nakamura, T., 2023. Development of preparation methods of polished sections of returned samples from asteroid Ryugu by the Hayabusa2 spacecraft. Meteorit. Planet. Sci. https://doi.org/10.1111/maps.14036.

Nicodemus, F.E., 1965. Directional reflectance and emissivity of an opaque surface. Appl. Opt. 4, 767.

Noguchi, T., Matsumoto, T., Miyake, A., Igami, Y., Haruta, M., Saito, H., Hata, S., Seto, Y., Miyahara, M., Tomioka, N., Ishii, H.A., Bradley, J.P., Ohtaki, K.K., Dobrică, E., Leroux, H., Le Guillou, C., Jacob, D., La Peña, F.de, Laforet, S., Marinova, M., Langenhorst, F., Harries, D., Beck, P., Phan, T.H.V., Rebois, R., Abreu, N.M., Gray, J., Zega, T., Zanetta, P.-M., Thompson, M.S., Stroud, R., Burgess, K., Cymes, B.A., Bridges, J.C., Hicks, L., Lee, M.R., Daly, L., Bland, P.A., Zolensky, M.E., Frank, D.R., Martinez, J., Tsuchiyama, A., Yasutake, M., Matsuno, J., Okumura, S., Mitsukawa, I., Uesugi, K., Uesugi, M., Takeuchi, A., Sun, M., Enju, S., Takigawa, A., Michikami, T., Nakamura, T., Matsumoto, M., Nakauchi, Y., Abe, M., Arakawa, M., Fujii, A., Hayakawa, M., Hirata, N., Hirata, N., Honda, R., Honda, C., Hosoda, S., Iijima, Y.-I., Ikeda, H., Ishiguro, M., Ishihara, Y., Iwata, T., Kawahara, K., Kikuchi, S., Kitazato, K., Matsumoto, K., Matsuoka, M., Mimasu, Y., Miura, A., Morota, T., Nakazawa, S., Namiki, N., Noda, H., Noguchi, R., Ogawa, N., Ogawa, K., Okada, T., Okamoto, C., Ono, G., Ozaki, M., Saiki, T., Sakatani, N., Sawada, H., Senshu, H., Shimaki, Y., Shirai, K., Sugita, S., Takei, Y., Takeuchi, H., Tanaka, S., Tatsumi, E., Terui, F., Tsukizaki, R., Wada, K., Yamada, M., Yamada, T., Yamamoto, Y., Yano, H., Yokota, Y., Yoshihara, K., Yoshikawa, M., Yoshikawa, K., Fukai, R., Furuya, S., Hatakeda, K., Hayashi, T., Hitomi, Y., Kumagai, K., Miyazaki, A., Nakato, A., Nishimura, M., Soejima, H., Suzuki, A.I., Usui, T., Yada, T., Yamamoto, D., Yogata, K., Yoshitake, M., Connolly, H.C., Lauretta, D.S., Yurimoto, H., Nagashima, K., Kawasaki, N., Sakamoto, N., Okazaki, R., Yabuta, H., Naraoka, H., Sakamoto, K., Tachibana, S., Watanabe, S., Tsuda, Y., 2023. A dehydrated space-weathered skin cloaking the hydrated interior of Ryugu. Nat. Astron. 7, 170–181.

Osawa, T., Kagi, H., Nakamura, T., Noguchi, T., 2005. Infrared spectroscopic taxonomy for carbonaceous chondrites from speciation of hydrous components. MAPS 40, 71–86.

Palme, H., Lodders, K., Jones, A., 2014. Solar system abundances of the elements. In: Treatise on Geochemistry. Elsevier, pp. 15–36.

Palomba, E., Longobardo, A., De Sanctis, Stein, N.T., Ehlmann, B., Galiano, A., Raponi, A., Ciarniello, M., Ammannito, E., Cloutis, E., Carrozzo, F.G., Capria, M.T., Stephan, K., Zambon, F., Tosi, F., Raymond, C.A., Russell, C.T., 2019. Compositional differences among Bright Spots on the Ceres surface. Icarus 320, 202–212.

Patzek, M., Bischoff, A., Visser, R., John, T., 2018. Mineralogy of volatile-rich clasts in brecciated meteorites. MAPS 53, 2519–2540.

Patzek, M., Hoppe, P., Bischoff, A., Visser, R., John, T., 2020. Hydrogen isotopic composition of CI- and CM-like clasts from meteorite breccias – sampling unknown sources of carbonaceous chondrite materials. GCA 272, 177–197.

Prencipe, M., Pascale, F., Zicovich-Wilson, C.M., Saunders, V.R., Orlando, R., Dovesi, R., 2004. The vibrational spectrum of calcite (CaCO3): an ab initio quantum-mechanical calculation. Phys. Chem. Miner. 31, 559–564.

Reddy, V., Dunn, T.L., Thomas, C.A., Moskovitz, N.A., Burbine, T.H., 2015. Mineralogy and surface composition of asteroids. In: Michel, P., DeMeo, F.E., Bottke, W.F. (Eds.), Asteroids IV. University of Arizona Press.

Reitze, M.P., Weber, I., Kroll, H., Morlok, A., Hiesinger, H., Helbert, J., 2020. Mid-infrared spectroscopy of alkali feldspar samples for space application. Mineral. Petrol. 114, 453–463.

Reitze, M.P., Weber, I., Morlok, A., Hiesinger, H., Bauch, K.E., Stojic, A.N., Helbert, J., 2021. Mid-infrared spectroscopy of crystalline plagioclase feldspar samples with various Al,Si order and implications for remote sensing of Mercury and other terrestrial Solar System objects. EPSL 554, 116697.

Saiki, T., Imamura, H., Arakawa, M., Wada, K., Takagi, Y., Hayakawa, M., Shirai, K., Yano, H., Okamoto, C., 2017. The small carry-on impactor (SCI) and the Hayabusa2 impact experiment. Space Sci. Rev. 208, 165–186.

Sakatani, N., Tanaka, S., Okada, T., Fukuhara, T., Riu, L., Sugita, S., Honda, R., Morota, T., Kameda, S., Yokota, Y., Tatsumi, E., Yumoto, K., Hirata, N., Miura, A., Kouyama, T., Senshu, H., Shimaki, Y., Arai, T., Takita, J., Demura, H., Sekiguchi, T., Müller, T.G., Hagermann, A., Biele, J., Grott, M., Hamm, M., Delbo, M., Neumann, W., Taguchi, M., Ogawa, Y., Matsunaga, T., Wada, T., Hasegawa, S., Helbert, J., Noguchi, R., Yamada, M., Suzuki, H., Honda, C., Ogawa, K., Hayakawa, M., Yoshioka, K., Matsuoka, M., Cho, Y., Sawada, H., Kitazato, K., Iwata, T., Abe, M., Ohtake, M., Matsuura, S., Matsumoto, K., Noda, H., Ishihara, Y., Yamamoto, K., Higuchi, A., Namiki, N., Ono, G., Saiki, T., Imamura, H., Takagi, Y., Yano, H., Shirai, K., Okamoto, C., Nakazawa, S., Iijima, Y., Arakawa, M., Wada, K., Kadono, T., Ishibashi, K., Terui, F., Kikuchi, S., Yamaguchi, T., Ogawa, N., Mimasu, Y., Yoshikawa, K., Takahashi, T., Takei, Y., Fujii, A., Takeuchi, H., Yamamoto, Y., Hirose, C., Hosoda, S., Mori, O., Shimada, T., Soldini, S., Tsukizaki, R., Ozaki, M., Tachibana, S., Ikeda, H., Ishiguro, M., Yabuta, H., Yoshikawa, M., Watanabe, S., Tsuda, Y., 2021. Anomalously porous boulders on (162173) Ryugu as primordial materials from its parent body. Nat. Astron. 5, 766–774.

Salisbury, J.W., Wald, A., 1992. The role of volume scattering in reducing spectral contrast of Reststrahlen bands in spectra of powdered minerals. Icarus 96 (1), 121–128.

Salisbury, J.W., Hapke, B., Eastes, J.W., 1987. Usefulness of weak bands in midinfrared remote sensing of particulate planetary surfaces. J. Geophys. Res. 92, 702.

Salisbury, J.W., D'Aria, D.M., Jarosewich, E., 1991. Midinfrared (2.5–13.5 μm) reflectance spectra of powdered stony meteorites. Icarus 92, 280–297.

Salisbury, J.W., Basu, A., Fischer, E.M., 1997. Thermal infrared spectra of lunar soils. Icarus 130 (1), 125–139.

Schönbächler, M., Carlson, R.W., Horan, M.F., Mock, T.D., Hauri, E.H., 2010. Heterogeneous accretion and the moderately volatile element budget of Earth. Science (New York, N.Y.) 328, 884–887.

Simon, A.A., Kaplan, H.H., Hamilton, V.E., Lauretta, D.S., Campins, H., Emery, J.P., Barucci, M.A., DellaGiustina, D.N., Reuter, D.C., Sandford, S.A., Golish, D.R., Lim, L. F., Ryan, A., Rozitis, B., Bennett, C.A., 2020. Widespread carbon-bearing materials on near-earth asteroid (101955) Bennu. Science 370.

Skulteti, A., Kereszturi, A., Szabo, M., Kereszty, Z., Cipriani, F., 2020. Mid-infrared spectroscopic investigation of meteorites and perspectives for thermal infrared observations at the binary asteroid Didymos. Planet. Space Sci. 184, 104855.

Stojic, A.N., Morlok, A., Tollan, P., Kohout, T., Hermann, J., Weber, I., Moreau, J.-G., Hiesinger, H., Sohn, M., Bauch, K.E., Reitze, M.P., Helbert, J., 2021. A shock recovery experiment and its implications for Mercury's surface: the effect of high pressure on porous olivine powder as a regolith analog. Icarus 357, 114162.

Sugita, S., Honda, R., Morota, T., Kameda, S., Sawada, H., Tatsumi, E., Yamada, M., Honda, C., Yokota, Y., Kouyama, T., Sakatani, N., Ogawa, K., Suzuki, H., Okada, T., Namiki, N., Tanaka, S., Iijima, Y., Yoshioka, K., Hayakawa, M., Cho, Y., Matsuoka, M., Hirata, N., Miyamoto, H., Domingue, D., Hirabayashi, M., Nakamura, T., Hiroi, T., Michikami, T., Michel, P., Ballouz, R.-L., Barnouin, O.S., Ernst, C.M., Schröder, S.E., Kikuchi, H., Hemmi, R., Komatsu, G., Fukuhara, T., Taguchi, M., Arai, T., Senshu, H., Demura, H., Ogawa, Y., Shimaki, Y., Sekiguchi, T., Müller, T.G., Hagermann, A., Mizuno, T., Noda, H., Matsumoto, K., Yamada, R., Ishihara, Y., Ikeda, H., Araki, H., Yamamoto, K., Abe, S., Yoshida, F., Higuchi, A., Sasaki, S., Oshigami, S., Tsuruta, S., Asari, K., Tazawa, S., Shizugami, M., Kimura, J., Otsubo, T., Yabuta, H., Hasegawa, S., Ishiguro, M., Tachibana, S., Palmer, E., Gaskell, R., Le Corre, L., Jaumann, R., Otto, K., Schmitz, N., Abell, P.A., Barucci, M. A., Zolensky, M.E., Vilas, F., Thuillet, F., Sugimoto, C., Takaki, N., Suzuki, Y., Kamiyoshihara, H., Okada, M., Nagata, K., Fujimoto, M., Yoshikawa, M., Yamamoto, Y., Shirai, K., Noguchi, R., Ogawa, N., Terui, F., Kikuchi, S., Yamaguchi, T., Oki, Y., Takao, Y., Takeuchi, H., Ono, G., Mimasu, Y., Yoshikawa, K., Takahashi, T., Takei, Y., Fujii, A., Hirose, C., Nakazawa, S., Hosoda, S., Mori, O., Shimada, T., Soldini, S., Iwata, T., Abe, M., Yano, H., Tsukizaki, R., Ozaki, M., Nishiyama, K., Saiki, T., Watanabe, S., Tsuda, Y., 2019. The geomorphology, color, and thermal properties of Ryugu: implications for parent-body processes. Science 364, 252.

Takir, D., Emery, J.P., 2012. Outer Main Belt asteroids: identification and distribution of four 3-μm spectral groups. Icarus 219, 641–654.

Takir, D., Emery, J.P., McSween, Hibbitts, C.A., Clark, R.N., Pearson, N., Wang, A., 2013. Nature and degree of aqueous alteration in CM and CI carbonaceous chondrites. Meteoritics & Planetary Science 48 (9), 1618–1637.

Takir, D., Emery, J.P., McSween, H.Y., 2015. Toward an understanding of phyllosilicate mineralogy in the outer main asteroid belt. Icarus 257, 185–193.

Tedesco, E.F., Williams, J.G., Matson, D.L., Weeder, G.J., Gradie, J.C., Lebofsky, L.A., 1989. A three-parameter asteroid taxonomy. Astron. J. 97, 580.

Tholen, D.J., 1989. Asteroid taxonomic classifications. In: Asteroids II. Arizona Press, Tucson, pp. 1139–1150.

Tholen, D.J., Barucci, M.A., 1989. Asteroid taxonomy. In: Asteroids II. Univ. of Arizona Press, Tucson, Ariz, pp. 298–315.

Tomeoka, K., Buseck, P.R., 1988. Matrix mineralogy of the Orgueil CI carbonaceous chondrite. GCA 52, 1627–1640.

Vernazza, P., Marsset, M., Beck, P., Binzel, R.P., Birlan, M., Brunetto, R., DeMeo, F.E., Djouadi, Z., Dumas, C., Merouane, S., Mousis, O., Zanda, B., 2015. Interplanetary dust particles as samples of icy asteroids. ApJ 806, 204.

Visser, R., John, T., Menneken, M., Patzek, M., Bischoff, A., 2018. Temperature constraints by Raman spectroscopy of organic matter in volatile-rich clasts and carbonaceous chondrites. GCA 241, 38–55.
Visser, R., John, T., Patzek, M., Bischoff, A., Whitehouse, M.J., 2019. Sulfur isotope study of sulfides in CI, CM, C2ung chondrites and volatile-rich clasts – evidence for different generations and reservoirs of sulfide formation. GCA 261, 210–223.
Visser, R., John, T., Whitehouse, M.J., Patzek, M., Bischoff, A., 2020. A short-lived 26Al induced hydrothermal alteration event in the outer solar system: constraints from Mn/Cr ages of carbonates. EPSL 547, 116440.
Xu, S., Binzel, R.P., Burbine, T.H., Bus, S.J., 1995. Small Main-Belt asteroid spectroscopic survey: initial results. Icarus 115, 1–35.
Yada, T., Abe, M., Okada, T., Nakato, A., Yogata, K., Miyazaki, A., Hatakeda, K., Kumagai, K., Nishimura, M., Hitomi, Y., Soejima, H., Yoshitake, M., Iwamae, A., Furuya, S., Uesugi, M., Karouji, Y., Usui, T., Hayashi, T., Yamamoto, D., Fukai, R., Sugita, S., Cho, Y., Yumoto, K., Yabe, Y., Bibring, J.-P., Pilorget, C., Hamm, V., Brunetto, R., Riu, L., Lourit, L., Loizeau, D., Lequertier, G., Moussi-Soffys, A., Tachibana, S., Sawada, H., Okazaki, R., Takano, Y., Sakamoto, K., Miura, Y.N., Yano, H., Ireland, T.R., Yamada, T., Fujimoto, M., Kitazato, K., Namiki, N., Arakawa, M., Hirata, N., Yurimoto, H., Nakamura, T., Noguchi, T., Yabuta, H., Naraoka, H., Ito, M., Nakamura, E., Uesugi, K., Kobayashi, K., Michikami, T., Kikuchi, H., Hirata, N., Ishihara, Y., Matsumoto, K., Noda, H., Noguchi, R., Shimaki, Y., Shirai, K., Ogawa, K., Wada, K., Senshu, H., Yamamoto, Y., Morota, T., Honda, R., Honda, C., Yokota, Y., Matsuoka, M., Sakatani, N., Tatsumi, E., Miura, A., Yamada, M., Fujii, A., Hirose, C., Hosoda, S., Ikeda, H., Iwata, T., Kikuchi, S., Mimasu, Y., Mori, O., Ogawa, N., Ono, G., Shimada, T., Soldini, S., Takahashi, T., Takei, Y., Takeuchi, H., Tsukizaki, R., Yoshikawa, K., Terui, F., Nakazawa, S., Tanaka, S., Saiki, T., Yoshikawa, M., Watanabe, S., Tsuda, Y., 2022. Preliminary analysis of the Hayabusa2 samples returned from C-type asteroid Ryugu. Nat. Astron. 6, 214–220.
Yokoyama, T., Nagashima, K., Nakai, I., Young, E.D., Abe, Y., Aléon, J., Alexander, C.M. O., Amari, S., Amelin, Y., Bajo, K.-I., Bizzarro, M., Bouvier, A., Carlson, R.W., Chaussidon, M., Choi, B.-G., Dauphas, N., Davis, A.M., Di Rocco, T., Fujiya, W., Fukai, R., Gautam, I., Haba, M.K., Hibiya, Y., Hidaka, H., Homma, H., Hoppe, P., Huss, G.R., Ichida, K., Iizuka, T., Ireland, T.R., Ishikawa, A., Ito, M., Itoh, S., Kawasaki, N., Kita, N.T., Kitajima, K., Kleine, T., Komatani, S., Krot, A.N., Liu, M.-C., Masuda, Y., McKeegan, K.D., Morita, M., Motomura, K., Moynier, F., Nguyen, A., Nittler, L., Onose, M., Pack, A., Park, C., Piani, L., Qin, L., Russell, S.S., Sakamoto, N., Schönbächler, M., Tafla, L., Tang, H., Terada, K., Terada, Y., Usui, T., Wada, S., Wadhwa, M., Walker, R.J., Yamashita, K., Yin, Q.-Z., Yoneda, S., Yui, H., Zhang, A.-C., Connolly, H.C., Lauretta, D.S., Nakamura, T., Naraoka, H., Noguchi, T., Okazaki, R., Sakamoto, K., Yabuta, H., Abe, M., Arakawa, M., Fujii, A., Hayakawa, M., Hirata, N., Hirata, N., Honda, R., Honda, C., Hosoda, S., Iijima, Y.-I., Ikeda, H., Ishiguro, M., Ishihara, Y., Iwata, T., Kawahara, K., Kikuchi, S., Kitazato, K., Matsumoto, K., Matsuoka, M., Michikami, T., Mimasu, Y., Miura, A., Morota, T., Nakazawa, S., Namiki, N., Noda, H., Noguchi, R., Ogawa, N., Ogawa, K., Okada, T., Okamoto, C., Ono, G., Ozaki, M., Saiki, T., Sakatani, N., Sawada, H., Senshu, H., Shimaki, Y., Shirai, K., Sugita, S., Takei, Y., Takeuchi, H., Tanaka, S., Tatsumi, E., Terui, F., Tsuda, Y., Tsukizaki, R., Wada, K., Watanabe, S., Yamada, M., Yamada, T., Yamamoto, Y., Yano, H., Yokota, Y., Yoshihara, K., Yoshikawa, M., Yoshikawa, K., Furuya, S., Hatakeda, K., Hayashi, T., Hitomi, Y., Kumagai, K., Miyazaki, A., Nakato, A., Nishimura, M., Soejima, H., Suzuki, A., Yada, T., Yamamoto, D., Yogata, K., Yoshitake, M., Tachibana, S., Yurimoto, H., 2023. Samples returned from the asteroid Ryugu are similar to Ivuna-type carbonaceous meteorites. Science 379, eabn7850.
Zolensky, M., Barrett, R., Browning, L., 1993. Mineralogy and composition of matrix and chondrule rims in carbonaceous chondrites. GCA 57, 3123–3148.
Zolensky, M.E., Weisberg, M.K., Buchanan, P.C., Mittlefehldt, D.W., 1996. Mineralogy of carbonaceous chondrite clasts in HED achondrites and the Moon. MAPS 31, 518–537.